High-Nuclearity Close-Packed Palladium-Nickel Carbonyl Phosphine Clusters: Heteropalladium $[Pd_{16}Ni_4(CO)_{22}(PPh_3)_4]^{2-}$ and $[Pd_{33}Ni_9(CO)_{41}(PPh_3)_6]^{4-}$ Containing Pseudo-T_d ccp $Pd_{16}Ni_4$ and Pseudo-D_{3h} hcp $Pd_{33}Ni_9$ Cores

Masaki Kawano,[1a] Jeffrey W. Bacon,[1a] Charles F. Campana,[1b] Brian E. Winger,[1c] James D. Dudek,[1d] Scott A. Sirchio,[1d] Sabrina L. Scruggs,[1d] Urs Geiser,[1d] and Lawrence F. Dahl*,[1a]

Department of Chemistry, University of Wisconsin-Madison, 1101 University Avenue, Madison, Wisconsin 53706, Bruker Analytical X-ray Systems, Inc., 5465 East Cheryl Parkway, Madison, Wisconsin 53711-5373, Finnigan FT/MS Corporation, 6416 Schroeder Road, Madison, Wisconsin 53711, and Chemistry and Materials Science Divisions, Argonne National Laboratory, 9700 South Cass Avenue, Argonne, Illinois 60439

Received August 25, 2000

$[Pd_{16}Ni_4(CO)_{22}(PPh_3)_4]^{2-}$ (**1**) and $[Pd_{33}Ni_9(CO)_{41}(PPh_3)_6]^{4-}$ (**2**) were obtained as the two major products from the reduction of $PdCl_2(PPh_3)_2$ with $[Ni_6(CO)_{12}]^{2-}$. Their crystal structures as $[PPh_4]^+$ salts were unambiguously determined from CCD X-ray crystallographic analyses; the resulting stoichiometries were ascertained from elemental analyses. Infrared, multinuclear ^1H, $^{31}P\{^1H\}$ NMR, UV−vis, CV, variable-temperature magnetic susceptibility, and ESI FT/ICR mass spectrometric measurements were performed. The $Pd_{16}Ni_4$ core of **1** ideally conforms to a ccp ν_3 tetrahedron of pseudo-T_d ($\bar{4}3m$) symmetry. Its geometry normal to each tetrahedral Pd_7Ni_3 face (i.e., along each of the four 3-fold axes) may be viewed as a four-layer stacking of 20 metal atoms in a ccp [a(Ni_1) b(Pd_3) c(Pd_6) a(Pd_7Ni_3)] sequence. A comparative analysis of the different ligand connectivities about the analogous metal-core geometries in **1** and the previously reported $[Os_{20}(CO)_{40}]^{2-}$ has stereochemical implications pertaining to the different possible modes of carbon monoxide attachment to ccp metal(111) surfaces. The unique geometry of the $Pd_{33}Ni_9$ core of **2**, which has pseudo-D_{3h} ($\bar{6}2m$) symmetry, consists of five equilateral triangular layers that are stacked in a hcp [a(Pd_7Ni_3) b(Pd_6) a(Pd_7Ni_3) b(Pd_6) a(Pd_7Ni_3)] sequence. Variable-temperature magnetic susceptibility measurements indicated both **1** and **2** to be diamagnetic over the entire temperature range from 5.0 to 300 K. Neutral $Pd_{12}(CO)_{12}(PPh_3)_6$ (**3**) and $[Pd_{29}(CO)_{28}(PPh_3)_7]^{2-}$ (**4**) as the $[PPh_4]^+$ salt were obtained as minor decomposition products from protonation reactions of **1** and **2**, respectively, with acetic acid. Compound **3** of pseudo-D_{3d} ($\bar{3}2/m$) symmetry represents the second highly deformed hexacapped octahedral member of the previously established homopalladium family of clusters containing uncapped, monocapped, bicapped, and tetracapped Pd_6 octahedra. The unprecedented centered 28-atom polyhedron for the Pd_{29} core of **4** of pseudo-C_{3v} (3m) symmetry may be described as a four-layer stacking of 29 metal atoms in a mixed hcp/ccp [a(Pd_1) b(Pd_3) a(Pd_{10}) c(Pd_{15})] sequence.

Introduction

During the last several years a considerable part of our research has focused on the preparation, isolation, crystallization, and stereophysical characterization of new high-nuclearity close-packed homopalladium and heteropalladium carbonyl clusters that possess direct metal−metal bonding interactions.[2] Such transition-metal clusters (arbitrarily defined by us to contain a minimum of 10 metal atoms) are of particular significance in that they fall in the intermediate metal-size range between the extreme limits of complexes with individual metal atoms and bulk metals. Hence, detailed studies of their physical properties should provide insight concerning the reported onset of metallic-like properties due to quantum-size effects with increasing metal cluster size that have been proposed for other high-nuclearity metal clusters.[3] Palladium as bulk metal or contained in compounds, alloys, and clusters is widely utilized as heterogeneous/homogeneous catalysts[4] or as catalytic precursors[5a] in many organic reactions. For example, the role of palladium in

(1) (a) UW-Madison. (b) Bruker Analytical X-ray Systems, Inc. (c) Finnigan FT/MS Corporation (d) Argonne National Laboratory.

(2) (a) Kawano, M.; Bacon, J. W.; Campana, C. F.; Dahl, L. F. *J. Am. Chem. Soc.* **1996**, *118*, 7869. (b) Bemis, J. M.; Dahl, L. F. *J. Am. Chem. Soc.* **1997**, *119*, 4545. (c) Tran, N. T.; Kawano, M.; Powell, D. R.; Dahl, L. F. *J. Am. Chem. Soc.* **1998**, *120*, 10986. (d) Tran, N. T.; Kawano, M.; Powell, D. R.; Hayashi, R. K.; Campana, C. F.; Dahl, L. F. *J. Am. Chem. Soc.* **1999**, *121*, 5945.

(3) (a) de Jongh, L. J. In *Physics and Chemistry of Metal Cluster Compounds*; de Jongh, L. J., Ed.; Kluwer Academic Publishers: The Netherlands, 1994; Chapter 1, pp 1−39. (b) Brom, H. B.; Baak, J.; de Jongh, L. J. In *Physics and Chemistry of Metal Cluster Compounds*; de Jongh, L. J., Ed.; Kluwer Academic Publishers: The Netherlands, 1994; Chapter 7, pp 211−226. (c) Brom, H. B.; van der Putten, D.; de Jongh, L. J. In *Physics and Chemistry of Metal Cluster Compounds*; de Jongh, L. J., Ed.; Kluwer Academic Publishers: The Netherlands, 1994; Chapter 8, pp 227−247. (d) Benfield, R. E. In *Physics and Chemistry of Metal Cluster Compounds*; de Jongh, L. J., Ed.; Kluwer Academic Publishers: The Netherlands, 1994; Chapter 9, pp 249−275. (e) Van Ruitenbeek, J. M.; Van Leeuwen, D. A.; de Jongh, L. J. In *Physics and Chemistry of Metal Cluster Compounds*; de Jongh, L. J., Ed.; Kluwer Academic Publishers: The Netherlands, 1994; Chapter 10, pp 277−306. (f) Benfield, R. E. *J. Phys. Chem.* **1987**, *91*, 2712 and references therein. (g) Volokitin, Y.; Sinzig, J.; de Jongh, L. J.; Schmid, G.; Vargaftik, M. N.; Moiseev, I. I. *Nature* **1996**, *384*, 621. (h) de Jongh, L. J. *J. Appl. Organomet. Chem.* **1998**, *12*, 393 and references therein.

10.1021/ic000979p CCC: $20.00
Published on Web 04/24/2001

automobile exhaust catalysts involving surface interactions with CO and NO is of importance.[5b] In addition, palladium metal has been utilized for tritium storage, purification, and isotope separation for at least 20 years.[6] Palladium is the only late transition metal (Groups 8−10) that does not form stable, discrete pure homometallic carbonyl clusters.[7,8] However, solution-phase palladium carbonyl complexes can be prepared with other stabilizing ligands,[9a,b] and CO readily absorbs on palladium surfaces.[9c] In addition, gas-phase $[Pd_3(CO)_n]^-$ anions ($n = 1-6$) have been generated, and their binding energies have been measured by the collision-induced dissociation method.[9d]

Our research on high-nuclearity heterometallic clusters containing palladium[10] has particular relevance to the many diverse experimental/theoretical investigations during the past decade on the preparation, characterization, and applications to catalysis of polymer-stabilized bimetallic nanoparticles,[11] especially those of Pd/Pt[12] and Pd/Ni.[13] The polymer-protected Pd/Ni nanoparticles were found to have a much higher catalytic activity for hydrogenation of nitrobenzene to aniline under mild conditions than monometallic Pd or Ni clusters.[13] A previous investigation[14] showed that Pd−Ni alloys supported on NaY zeolite exhibit significantly greater selectivity differences in CO hydrogenation compared with monometallic Pd/NaY and Ni/NaY samples and their physical mixtures. Moreover, combined experimental/theoretical studies[15] on Pd films over Ni(111) surfaces indicate significant electronic perturbation of the Pd atoms in accordance with marked changes in their catalytic properties, as illustrated by a striking catalytic efficiency in the hydrogenation of butadiene. An extensive theoretical examination of the electronic behavior of Ni, Pd, and Pt in overlayers of bimetallic surfaces[16] revealed an excellent correlation between electronic and physical/chemical properties induced by bimetallic bonding. One intriguing conclusion was that bimetallic bonding deactivates the Group 10 metals toward CO chemisorption.

In light of the above-mentioned activities and results on Pd/Ni nanoparticles, films, and alloys, we decided to carry out synthetic explorations designed to isolate well-defined high-nuclearity Pd−Ni carbonyl clusters in sufficient yields to allow investigations of their physical/chemical properties. This research was also motivated by the synthetic successes of Longoni, Ceriotti, and co-workers[17,18] in isolating and structurally/spectroscopically analyzing two highly remarkable series of high-nuclearity Pt−Ni carbonyl clusters, $[H_{6-n}Ni_{38}Pt_6(CO)_{48}]^{n-}$ ($n = 4, 5, 6$)[17] and $[H_{4-n}Ni_9Pt_3(CO)_{21}]^{n-}$ ($n = 3, 4$).[18] The first series of anions possesses a structurally unprecedented 44-atom ccp metal framework consisting of an octahedral Pt_6 kernel fully encapsulated by a ν_3 Ni_{38} octahedron.[17] For the second series of anions which are isostructural with those of the $[H_{2-n}Ni_{12}(CO)_{21}]^{(n+2)-}$ series ($n = 0, 1, 2$),[19] the metal framework is composed of three layers that are stacked in a hcp [a(Ni_3)b(Pt_3Ni_3)a(Ni_3)] sequence in which the three Pt atoms in the middle ν_2 Pt_3Ni_3 triangle occupy the inner triangle.[18] Recently, two new equally remarkable cocrystallized Pt−Ni carbonyl clusters, $[Pt_4Ni_{36}(CO)_{45}]^{6-}$ and $[Pt_4Ni_{37}(CO)_{46}]^{6-}$, were reported; each of these two crystallographically superimposed anions contains a Pt_4 tetrahedron encapsulated by an incomplete tetrahedron of Ni atoms.[20]

(4) (a) Moiseev, I. I.; Vargaftik, M. N. *New J. Chem.* **1998**, *22*, 1217. (b) *Catalysis by Di- and Polynuclear Metal Cluster Complexes*; Adams, R. D., Cotton, F. A., Eds.; Wiley-VCH: New York, 1998; pp 1−555. (c) Braunstein, P.; Rosé, J. In *Comprehensive Organometallic Chemistry II*; Abel, E. W., Stone, F. G. A., Wilkinson, G., Eds.; Elsevier: Tarrytown, NY, 1995; Vol. 10, Adams, R. D., Chapter Ed., Chapter 7, p 351. (d) Malleron, J.-L.; Fiaud, J. C.; Legros, J. Y. *Handbook of Palladium Catalysed Organic Reactions*; Academic Press: San Diego, CA, 1997. (e) Malleron, J.-L.; Juin, A. *Database of Palladium Chemistry*; Academic Press: San Diego, CA, 1997. (f) Sachtler, W. M. H.; Stakheev, A. Yu. *Catal. Today* **1992**, *12*, 283 and references therein. (g) Zhang, Z.; Cavalcanti, A. P.; Sachtler, W. M. H. *Catal. Lett.* **1992**, *12*, 157. (h) Zhang, Z.; Xu, L.; Sachtler, W. M. H. *J. Catal.* **1991**, *131*, 502. (i) Xu, L.; Lei, G. D.; Sachtler, W. M. H.; Cörtright, R. D.; Dumesic, J. A. *J. Phys. Chem.* **1993**, *97*, 11517 and references therein. (j) Sinfelt, J. H. *Bimetallic Catalysts: Discoveries, Concepts, and Applications*; John Wiley & Sons: New York, 1983 and references therein. (k) Gates, B. C. *Catalytic Chemistry*; John Wiley & Sons: New York, 1992. (i) *Metal Clusters in Chemistry*; Braunstein, P., Oro, L. A., Raithby, P. R., Eds.; Wiley-VCH: New York, 1999; Vol. 2. (l) *Handbook of Heterogeneous Catalysis*; Ertl, G., Knözinger, H., Weitkamp, J., Eds.; Wiley-VCH: New York, 1994.

(5) (a) Ichikawa, M. *Adv. Catal.* **1992**, *38*, 283 and references therein. (b) Kummer, J. T. *J. Phys. Chem.* **1986**, *90*, 4747 and references therein.

(6) Dr. Myung Lee (SRTC, Westinghouse Savannah River Company, Aiken, South Carolina), private communication to Dahl, L. F. August, 1995.

(7) Binary $[M(CO)_4]^{2+}$ dications (M = Pd, Pt) were isolated as white, thermally stable, crystalline salts.[8a] These unprecedented square-planar dications, which exhibit exceptionally high, virtually identical carbonyl stretching frequencies of 2260 cm^{-1} (av), are members of a small select group of so-called "nonclassical" metal carbonyl cations with normally higher carbonyl frequencies than that of 2143 for the gaseous (free) CO molecule.[8b,c] Although the M−CO bonding interactions for this entire class of homoleptic noble-metal carbonyl cations are attributed predominantly to σ-bonding only, ab initio electronic structure calculations instead indicate that electrostatic effects constitute the major factor responsible for these unusually high observed carbonyl frequencies and that C-to-M σ bonding donation is *not* important.[8d]

(8) (a) Hwang, G.; Wang, C.; Aubke, F.; Willner, H.; Bodenbinder, M. *Can. J. Chem.* **1993**, *71*, 1532. (b) Aubke, F.; Wang, C. *Coord. Chem. Rev.* **1994**, *137*, 483 and references therein. (c) Strauss, S. H. *J. Chem. Soc., Dalton Trans.* **2000**, 1 and references therein. (d) Goldman, A. S.; Krogh-Jespersen, K. *J. Am. Chem. Soc.* **1996**, *118*, 12159.

(9) (a) Stromnova, T. A.; Moiseev, I. I. *Russ. Chem. Rev.* **1998**, *67*, 485 and references therein. (b) Dixon, K. R.; Dixon, A. C. In *Comprehensive Organometallic Chemistry II*; Puddephatt, R. J., Ed.; Pergamon: London, 1995; Vol. 9, p 198 and references therein. (c) Yeo, Y. Y.; Vattuone, L.; King, D. A. *J. Chem. Phys.* **1997**, *106*, 1990 and references therein. (d) Spasov, V. A.; Ervin, K. M. *J. Chem. Phys.* **1998**, *109*, 5344.

(10) Lee, S.-M.; Wong, W.-T. *J. Cluster Sci.* **1998**, *9*, 417 and references therein.

(11) Toshima, N.; Yonezawa, T. *New J. Chem.* **1998**, *22*, 1179 and references therein.

(12) (a) Toshima, N.; Harada, M.; Yonezawa, T.; Kushihashi, K.; Asakura, K. *J. Phys. Chem.* **1991**, *95*, 7448. (b) Toshima, N.; Kushihashi, K.; Yonezawa, T.; Hirai, H. *Chem. Lett.* **1989**, 1769. (c) Toshima, N.; Yonezawa, T.; Kushihashi, K. *J. Chem. Soc., Faraday Trans.* **1993**, *89*, 2537. (d) Wang, Y.; Liu, H. *Polym. Bull.* **1991**, *25*, 139.

(13) (a) Toshima, N.; Lu, P. *Chem. Lett.* **1996**, 729. (b) Lu, P.; Teranishi, T.; Asakura, K.; Miyake, M.; Toshima, N. *J. Phys. Chem. B* **1999**, *103*, 9673.

(14) (a) Feeley, J. S.; Stakheev, A. Yu; Cavalcanti, A. P.; Sachtler, W. M. H., *J. Catal.* **1992**, *136*, 182. (b) Feeley, J. S.; Sachtler, W. M. H. *J. Catal.* **1991**, *131*, 573.

(15) (a) Bertolini, J. C.; Miegge, P.; Hermann, P.; Roussett, J. L.; Tardy, B. *Surf. Sci.* **1995**, *331*, 651. (b) Hermann, P.; Tardy, B.; Simon, D.; Guigner, J. M.; Bigot, B.; Bertolini, J. C. *Surf, Sci.* **1994**, *307*, 422. (c) Hermann, P.; Simon, D.; Bigot, B. *Surf. Sci.* **1996**, *350*, 301.

(16) (a) Rodriguez, J. A. *Surf. Sci.* **1996**, *345*, 347. (b) Rodriguez, J. A. *Heterog. Chem. Rev.* **1996**, *3*, 17. (c) Rodriguez, J. A. *Surf. Sci. Rep.* **1996**, *24*, 223. (d) Rodriguez, J. A.; Goodman, D. W. *Acc. Chem. Res.* **1995**, *28*, 477. (e) Rodriguez, J. A.; Goodman, D. W. *Science* **1992**, *257*, 897.

(17) (a) Ceriotti, A.; Demartin, F.; Longoni, G.; Manassero, M.; Marchionna, M.; Piva, G.; Sansoni, M. *Angew. Chem., Int. Ed. Engl.* **1985**, *24*, 697. (b) Fabrizi de Biani, F.; Femoni, C.; Iapalucci, M. C.; Longoni, G.; Zanello, P.; Ceriotti, A. *Inorg. Chem.* **1999**, *38*, 3721.

(18) Ceriotti, A.; Demartin, F.; Longoni, G.; Manassero, M.; Piva, G.; Piro, G.; Sansoni, M.; Heaton, B. T. *J. Organomet. Chem.* **1986**, *301*, C5.

(19) (a) $[Ni_{12}(CO)_{21}H_{4-n}]^{n-}$ ($n = 2, 3$): Broach, R. W.; Dahl, L. F.; Longoni, G.; Chini, P.; Schultz, A. J.; Williams, J. M. *Adv. Chem. Ser.* **1978**, *167*, 93. (b) $[Ni_{12}(CO)_{21}]^{4-}$ Chini, P.; Longoni, G.; Manassero, M.; Sansoni, M. *Abstracts of the Eighth Meeting of the Italian Association of Crystallography*; Ferrara, 1977; Communication 34. (c) $[Ni_{12}(CO)_{21}H_{4-n}]^{n-}$ ($n = 2-4$): Ceriotti, A.; Chini, P.; Pergola, R. D.; Longoni, G. *Inorg. Chem.* **1983**, *22*, 1595.

Unlike the Pt/Ni phase diagram which exhibits complete miscibility at high temperature but two intermetallic phases, NiPt and Ni_3Pt, at low temperatures,[21] the phase diagram for the Pd/Ni intermetallic system consists of a continuous solid solution at room temperature.[22] Therefore, it was of prime interest to determine whether complete or partial segregation of Pd and Ni occurs at the metal-core sites of any isolated and structurally determined bimetallic carbonyl cluster (i.e., whether there is crystallographic evidence of a substitutional Pd/Ni crystal disorder at a given metal-core site). We anticipated that the markedly different coordination behavior of carbonyl ligation between palladium and nickel might give rise to a well-defined Pd−Ni carbonyl phosphine cluster with a crystal-ordered Pd−Ni core (i.e., corresponding to only one stereoisomer).

Prior to our work, there was only one previously reported example of any discrete (Pd−Ni)-bonded heterometallic species: namely, $[PdNi_2(CNMe)_6(dppm)_2]^{2+}$ (as the $[PF_6]^-$ salt); its geometry consists of a centrosymmetrically required linear Ni−Pd−Ni unit with the central Pd having an approximately square-planar environment of two phosphorus and the two nickel atoms.[23] Furthermore, only a few structurally determined high-nuclearity heterometallic carbonyl clusters containing palladium were then known; these include the isostructural but electronically nonequivalent $[HPd_6Fe_6(CO)_{24}]^{3-}$ trianion[24,25] and $[Pd_6Ru_6(CO)_{24}]^{2-}$ dianion,[25] the $[Au_2Pd_{14}(CO)_9(PMe_3)_{11}]^{2+}$ dication,[26] and recently $Pd_6Os_5(CO)_{19}(dppm)_2$ and the electronically equivalent and structurally analogous $H_2Pd_6Os_5(CO)_{18}(dppm)_2$.[27] Particularly noteworthy was the use of SiO_2-supported $[HPd_6Fe_6(CO)_{24}]^{3-}$ to generate by decarbonylation a Pd−Fe bimetallic catalyst that displayed high selectivity toward methanol synthesis from CO/H_2 reactions.[28] After the research given here, the $[Pd_7Ni_{18}(CO)_{33}]^{4-}$ and $[Pd_{16}Ni_{16}(CO)_{40}]^{4-}$ tetraanions,[29a] the $[Pd_{13}Ni_{13}(CO)_{34}]^{4-}$ tetraanion,[29b] and the substitutionally disordered $[Pd_{19.2}Ni_{22.8}(CO)_{46}]^{6-}$ hexaanion[29c] have been prepared and structurally analyzed in our laboratory; a recent report by Longoni and co-workers[30] gives the preparation and crystallographic characterization of the $[Pd_{16}Ni_{16}(CO)_{40}]^{4-}$ tetraanion and $[Pd_{20}Ni_{26}(CO)_{54}]^{6-}$ hexaanion.

The research presented herein on the preparation, isolation, crystallization, structural/bonding analyses, and physical/chemical properties of two similarly remarkable palladium−nickel clusters, $[Pd_{16}Ni_4(CO)_{22}(PPh_3)_4]^{2-}$ (**1**) and $[Pd_{33}Ni_9(CO)_{41}(PPh_3)_6]^{4-}$ (**2**), was an outgrowth of previous synthetic explorations performed in our laboratory by Bacon.[31] Occasionally, Bacon isolated small quantities of crystalline products from his reactions that were designed to obtain Pd−Ni carbonyl clusters, but the crystals invariably were too small and/or weakly diffracting to even obtain lattice parameters via a conventional scintillation point-detector diffractometer. Fortunately, a new-generation SMART CCD area-detector X-ray diffractometer (for use with MoKα radiation) became available at that time. Bacon's subsequent X-ray examination of a few crystals, obtained from a room-temperature reaction of $Pd(OAc)_2$ with $[NMe_4]_2[Ni_6(CO)_{12}]$ in DMSO, resulted in diffraction data being obtained from only one crystal. Although the structural determination was severely limited by an estimated 70% decay in equivalent intensities during data collection from this crystal at room temperature (i.e., a low-temperature setup was not available at that time), the crystallographic results unambiguiously revealed the existence of a new 30-atom ccp metal-core geometry that conforms to one edge-truncation of a regular 35-atom ν_4 tetrahedron.[32] Our tentative formulation of the compound as $[PPh_4]_4[Pd_{16}Ni_{14}(CO)_{36}]$ was based upon the partially determined crystal structure, elemental analysis, and IR data. Extensive efforts to isolate and crystallize this compound again are as yet unsuccessful.

The fact that this initial endeavor clearly established the existence of a geometrically unprecedented high-nuclearity Pd−Ni carbonyl cluster (even though its exact composition is not known) intensified our preparative activities in this area, which led to the preparation and structural determination by Kawano of $[Pd_{16}Ni_4(CO)_{22}(PPh_3)_4]^{2-}$ (**1**) and $[Pd_{33}Ni_9(CO)_{41}(PPh_3)_6]^{4-}$ (**2**). Both **1** and **2** were obtained in yields as high as 63% and 24%, respectively, from the reduction of $PdCl_2(PPh_3)_2$ with the $[Ni_6(CO)_{12}]^{2-}$ dianion. The stoichiometries of both **1** and **2** as $[PPh_4]^+$ salts were established unequivocally from X-ray structural determinations and ascertained from elemental analyses. Infrared, ^1H, $^{31}P\{^1H\}$ NMR, UV−vis, variable-temperature magnetic susceptibility, electrospray ionization Fourier transform ion-cyclotron-resonance mass spectrometric (ESI FT/ICR/MS), and cyclic voltammetric (CV) measurements were carried out on each compound. A preliminary account of the synthesis and crystallographic determination of **2** has been reported.[2a]

The neutral molecular $Pd_{12}(CO)_{12}(PPh_3)_6$ (**3**) and $[Pd_{29}(CO)_{28}(PPh_3)_7]^{2-}$ (**4**) as $[PPh_4]^+$ salts were obtained as minor decomposition products from separate reactions designed to protonate **1** and **2**, respectively, with acetic acid. Both their nonhydrogen stoichiometries and atomic arrangements were unequivocally determined from X-ray crystallographic analyses. Although **3** and **4** were both obtained in very low yields such that further analyses were not performed, the structural/bonding features of each of these minor side-products are of stereochemical importance (vide infra).

The SMART CCD area-detector X-ray diffractometry system was found again to be an essential ingredient in the structural elucidation of these four clusters. In each case the observed CCD X-ray data were sufficiently plentiful and precise to allow complete structural determinations.[33]

(20) Demartin, F.; Femoni, C.; Iapalucci, M. C.; Longoni, G.; Macchi P. *Angew. Chem., Int. Ed. Engl.* **1999**, *38*, 531.
(21) (a) Nash, P.; Singleton, M. F. In *Phase Diagrams of Binary Nickel Alloys*; Nash, P., Ed.; ASM International: Materials Park, OH, 1991; pp 261−264 and references therein. (b) Hansen, M.; Anderko, K. In *Constitution of Binary Alloys*; McGraw-Hill: New York, 1958; pp 1031−1032 and references therein.
(22) (a) Nash, A.; Nash, P. In *Phase Diagrams of Binary Nickel Alloys*; Nash, P., Ed.; ASM International: Materials Park, OH 44073, 1991; pp 251−256, and references therein. (b) Hansen, M.; Anderko, K. In *Constitution of Binary Alloys*; McGraw-Hill: New York, 1958; pp 1029−1031, and references therein.
(23) Ni, J.; Fanwick, P. E.; Kubiak, C. P. *Inorg. Chem.* **1988**, *27*, 2020.
(24) Longoni, G.; Manassero, M.; Sansoni, M. *J. Am. Chem. Soc.* **1980**, *102*, 3242.
(25) Brivio, E.; Ceriotti, A.; Pergola, R. D.; Garlaschelli, L.; Demartin, F.; Manassero, M.; Sansoni, M.; Zanello, P.; Laschi, F.; Heaton, B. T. *J. Chem Soc., Dalton Trans.* **1994**, 3237.
(26) Copley, R. C. B.; Hill, C. M.; Mingos, D. M. P. *J. Cluster Sci.* **1995**, *6*, 71.
(27) Hui, J. W.-S.; Wong, W.-T. *J. Chem Soc., Chem. Commun.* **1997**, 2009.
(28) Kimura, T.; Fukuoka, A.; Fumagalli, A.; Ichikawa, M. *Catal. Lett.* **1989**, *2*, 227.
(29) (a) Kozee, M. A.; Dahl, L. F. manuscript in preparation. (b) Tran, N. T.; Kawano, M.; Powell, D. R.; Dahl, L. F. *J. Chem Soc., Dalton Trans.* **2000**, 4138. (c) Kawano, M.; Dahl, L. F. Manuscript in preparation.
(30) Femoni, C.; Iapalucci, M. C.; Longoni, G.; Svensson, P. H.; Wolowska, J. *Angew. Chem., Int. Ed. Engl.* **2000**, *39*, 1635.
(31) Bacon, J. W.; Dahl, L. F. Unpublished research.
(32) This unprecedented polyhedron containing one interior and 29 surface metal atoms may be formally derived from a regular 35-atom ν_4 tetrahedron with 5 missing atoms along one edge. This ν_4 edge-truncated tetrahedron of pseudo-C_{2v} symmetry has two 14-atom [5, 4, 3, 2] and two 10-atom [4, 3, 2, 1] tetrahedral faces.

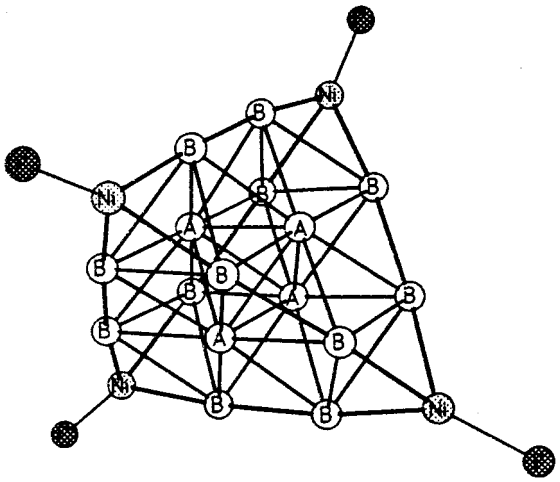

Figure 1. View of the 20-atom $Pd_{16}Ni_4$ core in $[Pd_{16}Ni_4(CO)_{22}(PPh_3)_4]^{2-}$ (**1**). Its metal-framework ideally conforms to a ccp ν_3 tetrahedron of T_d ($\bar{4}3m$) cubic symmetry with the four Ni atoms located at the tetrahedral corners. Its geometry normal to each of the four 3-fold axes may be described as a four-layer stacking of 20 metal atoms in a ccp [a(Ni_1) b(Pd_3) c(Pd_6) a(Pd_7Ni_3)] sequence. The four pseudoequivalent Pd(A) atoms are each located at the center of one of the four tetrahedral Pd_7Ni_3 faces, while the 12 pseudoequivalent Pd(B) atoms are distributed as the two internal metal atoms along each of the six tetrahedral Ni−Pd(B)−Pd(B)−Ni edges.

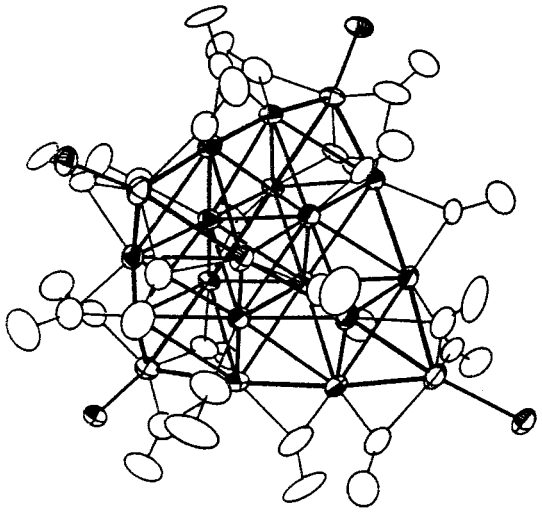

Figure 2. Configuration of $[Pd_{16}Ni_4(CO)_{22}(PPh_3)_4]^{2-}$ (**1**) without the phosphorus-attached phenyl substitutents. The connectivities of the four triphenyl phosphine P atoms, the four central Pd(A)-attached terminal COs, and the 18 edge-bridging COs spanning the three adjacent metal-atom pairs along each of the six tetrahedral Ni−Pd(B)−Pd(B)−Ni edges also conform to pseudo-T_d symmetry.

Results and Discussion

$[Pd_{16}Ni_4(CO)_{22}(PPh_3)_4]^{2-}$ Dianion (1). (a) Structural/Bonding Features. The architecture (Figure 1) of the 20-atom $Pd_{16}Ni_4$ core of **1**, which has crystallographic site symmetry C_1 (1), is best considered as a ccp ν_3 tetrahedron of pseudo-T_d symmetry with the four Ni atoms located at the four tetrahedral vertexes (i.e., the ν_n metal tetrahedron with $n = 3$ for **1** denotes that there are $n + 1 = 4$ metal atoms that are spaced along each of the six tetrahedral edges). The four equivalent tetrahedral faces are each composed of a 10-atom ν_2 triangular Pd_7Ni_3 layer with the three Ni atoms at the corners and the seven Pd atoms at the other positions of the equilateral triangle. Each of these faces represents a ccp (111) metal surface. Figure 1 reveals that under T_d symmetry the 16 Pd atoms consist of four equivalent Pd(A) and 12 equivalent Pd(B) atoms. The four Pd(A) atoms are each located at the center of one of the four tetrahedral Pd_7Ni_3 faces, while the 12 Pd(B) atoms are distributed in bonding pairs as the two internal metal atoms along each of the six tetrahedral Ni−Pd(B)−Pd(B)−Ni edges. The T_d $Pd_{16}Ni_4$ core may also be viewed along each of the four symmetry-equivalent 3-fold axes as a four-layer ccp fragment comprised of individual Ni_1, $Pd(B)_3$, $Pd(A)_3Pd(B)_3$, and $Ni_3Pd(A)Pd(B)_6$ layers.

Figure 2 gives a view of the dianion (excluding the phenyl substituents). The four triphenyl phosphine ligands are each coordinated to one of the four Ni atoms. The 22 carbonyl ligands consist of four terminal COs that are each linked to the central Pd(A) atom on one of the four tetrahedral Pd_7Ni_3 faces and 18 doubly bridging COs that span the three adjacent metal-atom pairs on each of the six tetrahedral Pd_2Ni_2 edges. Although the three doubly bridging COs along each edge are sterically disposed in zigzag arrangements to minimize nonbonding interactions, the resulting ligand connectivities are such that inclusion of the four P atoms (without the phenyl substituents) maintains the pseudo-T_d cubic symmetry of the $Pd_{16}Ni_4$ core. Each Ni atom, which is bonded to only three Pd(B) neighbors, has a tetrahedral-like ligand environment of one P and three bridging COs. Each Pd(A) atom, which has 9 nearest Pd neighbors (viz, six Pd(B) and three Pd(A) atoms) corresponding to the highest metal−metal connectivities, has only one attached terminal CO, whereas each Pd(B) atom, which has six nearest metal neighbors (viz, one Ni, two Pd(A), and three Pd(B) atoms), is also linked to two bridging COs. This inverse correlation in a ligated metal cluster between the number of metal connectivities to a given metal atom and the number of bound ligands is consistent with a theoretically based proposal[34a,b] that generally the number of cluster valence (CV) MOs available for ligand attachment in a close-packed metal cluster is inversely proportional to the number of nearest metal neighbors.

The entire $Pd_{16}Ni_4$ core contains four octahedra and 11 tetrahedra. The number and nature of these polyhedra become apparent if the 20-atom metal framework is perceived as a *supracluster*[35] that is comprised of a central $Pd(A)_4$ tetrahedron which is connected on each of its four tetrahedral faces to the triangular $Pd(B)_3$ face of a $NiPd(B)_3$ tetrahedron by trigonal-antiprismatic (pseudo-octahedral) capping. This condensation also involves each of the three Pd(B) atoms in the one $Pd(B)_3$ triangle of each $NiPd(B)_3$ tetrahedron being edge-linked to an

(33) A conventional point-detector Siemens P4 diffractometer along with a Mo rotating-anode system (50 kV, 200 mA) was initially used to obtain intensity data for **2** on the same crystal (for which periodic intensity-monitoring of standard reflections did not indicate any decay). A comparative analysis of the resulting scintillation point-detector data with the subsequent CCD area-detector data taken with a Mo sealed tube generator (50 kV, 40 mA) revealed the following striking differences: (1) time of data collection, 5 1/2 days vs 6 h; (2) scan speeds: 6−60°/min (ω scans) vs 10 s/frame (φ scans); (3) number of observed reflections ($I > 2\sigma(I)$; $3° < 2\theta < 45°$), 2, 814 vs 9, 918; (4) observed/independent data ratio, 15% vs 58%; (5) unweighted $R_1(F)$, 15% vs 11%. Despite the incident Mo Kα radiation from the rotating anode system being enhanced by a factor of ca. 4.0 relative to that for the stationary anode system, the very low number (15%) of observed data obtained from the scintillation point-detector system (compared to that of nearly 60% from the CCD system) gave rise to only the metal-core geometry of the $Pd_{33}Ni_9$ tetraanion (**2**) being resolved instead of the entire crystal structure.

(34) (a) Lauher, J. W. *J. Am. Chem. Soc.* **1978**, *100*, 5305. (b) Lauher, J. W. *J. Am. Chem. Soc.* **1979**, *101*, 2604. (c) Ciani, G.; Sironi, A. *J. Organomet. Chem.* **1980**, *197*, 233. (d) Lauher, J. W. *J. Organomet. Chem.* **1981**, *213*, 25.

(35) (a) Teo, B. K.; Zhang, H. *Inorg. Chem.* **1988**, *27*, 414. (b) Teo, B. K.; Zhang, H. *Inorg. Chim. Acta* **1988**, *144*, 173.

adjacent Pd(B) atom in another $Pd(B)_3$ triangle such that six $Pd(A)_2Pd(B)_2$ tetrahedra are concomitantly created along with six Ni−Pd(B)−Pd(B)−Ni edges corresponding to an overall ν_3 tetrahedral geometry. The $Pd_{16}Ni_4$ core may also be envisioned as a condensation product arising from the following: (1) the face-fusions of four Ni-capped $Pd(B)_3Pd(A)_3$ octahedra with a central $Pd(A)_4$ tetrahedron with attendant formation of the six additional Pd(B)−Pd(B) edge-connectivities; (2) the composite of four Ni-capped $Pd(B)_3Pd(A)_3$ octahedra sharing four Pd(A) vertexes (resulting in the linkage of each Pd(A) atom with three adjacent Ni-capped $Pd(B)_3Pd(A)_3$ octahedra) with accompanying formation of the six above-mentioned Pd(B)−Pd(B) edge-connectivities; or (3) the formal attachment of a 10-atom three-layer ν_2 $Ni/Pd_3/Pd_6$ tetrahedron along its Pd_6 face to a ν_3 Ni_3Pd_7 triangular layer.

The observed number of metal cluster valence electrons (CVEs) in this ccp tetrahedral cluster is 254 electrons (i.e., 16 × 10(Pd) + 4 × 10(Ni) + 22 × 2 (CO) + 4 × 2(PPh_3) + 2(charge) = 254). This observed number agrees closely with the predicted number of CVEs obtained from the Lauher/Ciani-Sironi model (254 electrons),[34,36] the Mingos model (252 electrons),[37,38] and the Teo-Zhang model (252 electrons)[39,40] for high-nuclearity metal clusters.

(b) Geometrical/Bonding Relationship with the $[Os_{20}(CO)_{40}]^{2-}$ Dianion (5). The only hitherto reported example established from an X-ray crystallographic analysis[41] of a metal cluster with the ccp ν_3 tetrahedral metal-core geometry is $[Os_{20}(CO)_{40}]^{2-}$ (**5**), for which its 20 metal atoms are enveloped by a ligand polyhedron of 40 terminal carbonyls. This monometallic cluster, prepared by Gade, Johnson, Lewis, and coworkers,[41] was thermolytically generated by vacuum pyrolysis of $Os_3(CO)_{10}(NCMe)_2$ in 20% yield along with the ν_2 tetrahedral $[Os_{10}C(CO)_{24}]^{2-}$, $[Os_{17}(CO)_{36}]^{2-}$, and other lower-nuclearity osmium species. The ν_3 tetrahedral metal skeleton of **5** (Figure 3) is formally derived from the ν_2 tetrahedral Os_{10} metal core found in the $[Os_{10}C(CO)_{24}]^{2-}$ dianion,[42a] the $[HOs_{10}C(CO)_{24}]^{-}$ monoanion,[42b] the neutral $H_2Os_{10}C(CO)_{24}$,[42c] and the $[H_4Os_{10}(CO)_{24}]^{2-}$ dianion[42d,e] by the addition of a planar equilateral triangle of 10 osmium atoms to the Os_6 face of the 3-layer Os_{10} tetrahedron. Although the observed valence electron count of 242 electrons based upon its formula is substantially less than the calculated values of 252 or 254 electrons from the electron-counting models (vide supra), no evidence was uncovered from IR, multinuclear ^1H and $^{13}C\{^1H\}$ NMR, and FAB mass spectrometric measurements for the possible presence of ad-

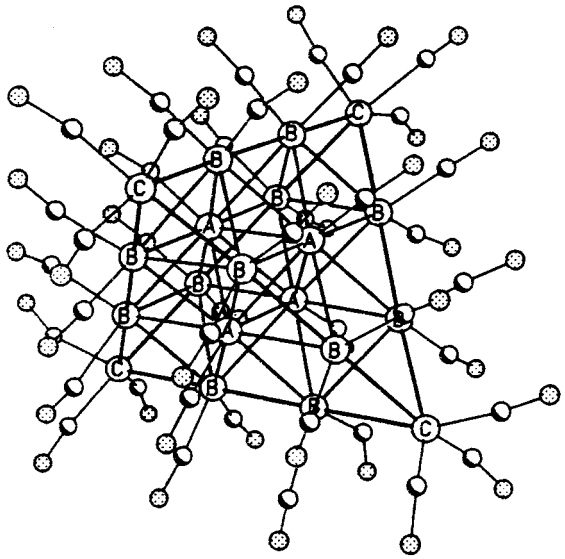

Figure 3. View of the known $[Os_{20}(CO)_{40}]^{2-}$ (**5**),[41] which has an analogous ccp ν_3 tetrahedral metal-core geometry as that of **1**. In sharp contrast with **1**, its 20 metal atoms are encapsulated by a pseudo T_d ligand polyhedron of 40 terminal COs. The different ligand connectivities about the common metal cores in **1** and **5** have stereochemical implications relating to the different possible modes of carbon monoxide attachment to ccp metal(111) surfaces.

(36) From extended Hückel MO calculations performed on a variety of ccp bare rhodium clusters including the 20-atom ν_3 tetrahedral metal geometry, Lauher[34a,b] determined the number of filled CVMOs for each geometry. For a corresponding ligated metal cluster with the same metal-core geometry he then presumed that if the metal atoms, the ligands, and the free charge give rise to the same number of filled CVMOs, the ligated metal cluster should be stable, irrespective of the actual metallic element or ligand disposition. For the ν_3 tetrahedral metal geometry, his calculations[34b] predicted the number of filled CVMOs to be 127 which corresponds to the number of CVEs being 254. Lauher[34b] estimated the bonding capabilities for each of the three different symmetry types of metal atoms in the 20-atom ν_3 tetrahedron that relate to the four Ni, four Pd(A), and 12 Pd(B) atoms in **1**. An extension of the Lauher approach by Ciani and Sironi[34c] to a large number of other compact close-packed bare rhodium clusters gave rise to the Ciani/Sironi rule that the number of filled CVMOs can be expressed as $6N + X$, where N is the number of metal atoms and X a variable depending upon the cluster geometry; for close-packed geometries or metal clusters with unknown geometries, an X value of 7 is normally used. The 20-atom T_d ν_3 metal tetrahedron in **1** has $X = 7$, resulting in the number of predicted CVEs being 254. The 42-atom D_{3h} metal core in **2** has $X = 7$, resulting in the number of predicted CVEs being 518. The D_{3d} Pd_{12} core in **3** has $X = 7$, resulting in the number of predicted CVEs being 158. The C_{3v} Pd_{29} core in **4** has $X = 7$, resulting in the number of predicted CVEs being 362.

(37) (a) Mingos, D. M. P. *J. Chem. Soc., Chem Commun.* **1985**, 1352. (b) Mingos, D. M. P.; Zhenyang, L. *J. Chem Soc., Dalton Trans.* **1988**, 1657.

(38) For high-nuclearity close-packed metal clusters, the Mingos model[37] presumes that the total valence electron count is given by $\Delta_i + 12n_s$, where Δ_i and n_s are the central fragment count and number of surface atoms, respectively. For the ccp $Pd_{16}Ni_4$ core in **1**, $\Delta_i = 60$ for the bonding $Pd(A)_4$ tetrahedron and $n_s = 16$; the resulting number of predicted CVEs is 252. For the hcp $Pd_{33}Ni_9$ core in **2**, $\Delta_i = 170$ for a centered 13-atom *anti*-cuboctahedron (hcp) and $n_s = 29$; the resulting number of predicted CVEs is 518. For the Pd_{12} core in **3**, $\Delta_i = 86$ for an octahedron and $n_s = 6$; the resulting number of predicted CVEs is 158. For the C_{3v} Pd_{29} core in **4**, $\Delta_i = 170$ for a centered cuboctahedron and $n_s = 16$; the resulting number of predicted CVEs is 362.

(39) (a) Teo, B. K.; Zhang, H. *Polyhedron* **1990**, *9*, 1985. (b) Teo, B. K.; Sloane, N. J. A. *Inorg. Chem.* **1986**, *25*, 2315. (c) Teo, B. K.; Sloane, N. J. A. *Inorg. Chem.* **1985**, *24*, 4545. (d) Sloane, N. J. A.; Teo, B. K. *J. Chem Phys.* **1985**, *83*, 6520.

(40) For a close-packed high-nuclearity metal cluster, the calculated electron count given by the Teo-Zhang model[39] is $2T_n = 2(6S_n + B_n)$, where T_n denotes the total number of topological electron pairs, S_n the total number of surface atoms, and B_n the number of shell electron-pairs. Alternatively, the same number of CVEs can be obtained from $2T_n = 2(6G_n + K)$, where G_n designates the total number of atoms and K is related to the B value at the cluster center. For the ccp $Pd_{16}Ni_4$ core in **1**, $S_n = 20$, $B_n = 6$, $G_n = 20$, and $K = 6$; for either of the above formulas the number of predicted CVEs is 252. For the hcp $Pd_{33}Ni_9$ core in **2**, $S_n = 41$, $B_n = 13$, $G_n = 42$, and $K = 7$; the resulting number of predicted CVEs is 518. For the D_{3d} Pd_{12} core in **3**, $S_n = 12$, $B_n = 7$, $G_n = 12$, and $K = 7$; the resulting number of predicted CVEs is 158. For the C_{3v} Pd_{29} core in **4**, $S_n = 28$, $B_n = 13$, $G_n = 29$, and $K = 7$; the resulting number of predicted CVEs is 362.

(41) (a) Amoroso, A. J.; Gade, L. H.; Johnson, B. F. G.; Lewis, J.; Raithby, P. R.; Wong, W.-T. *Angew. Chem., Int. Ed. Engl.* **1991**, *30*, 107. (b) Gade, L. H.; Johnson, B. F. G.; Lewis, J.; McPartlin, M. J.; Powell, H. R.; Raithby, P. R.; Wong, W.-T. *J. Chem. Soc., Dalton Trans*. **1994**, 521.

(42) (a) Jackson, P. F.; Johnson, B. F. G.; Lewis, J.; Nelson, W. J. H.; McPartlin M. J. *J. Chem. Soc., Dalton Trans*. **1982**, 2099. (b) Jackson, P. F.; Johnson, B. F. G.; Lewis, J.; McPartlin, M. J.; Nelson, W. J. H. *J. Chem. Soc., Chem. Commun*. **1982**, 49. (c) Braga, D.; Grepioni, F.; Righi, S.; Johnson, B. F. G.; Frediani, P.; Bianchi, M.; Piacenti, F.; Lewis, J. *Organometallics* **1992**, *11*, 706. (d) Braga, D.; Lewis, J.; Johnson, B. F. G.; McPartlin, M.; Nelson, W. J. H.; Vargas, M. D. *J. Chem. Soc., Chem. Commun*. **1983**, 241. (e) Bashall, A.; Gade, L. H.; Lewis, J.; Johnson, B. F. G.; McIntrye, G. J.; McPartlin, M. *Angew. Chem., Int. Ed. Engl*. **1991**, *30*, 1164.

ditional interstitial H or C atoms.[41] The nonconformity of **5** to the electron-counting models may be a consequence of the relatively strong Os−Os bonding interactions (vide infra) that stabilize this highly symmetric cluster despite its presumed electron-deficiency.

From theoretical studies[43] the same ν_3 tetrahedral structure has also been proposed as a particularly stable closed-shell electronic configuration for the abundant bare alkali metal M_{20} clusters associated with the large 20-atom peaks that are observed via mass spectra of supersonic jet-expansion beams of alkali-metal gases.

Of interest is a comparative analysis between the ligand arrangements in **1** and **5** about the common metal core. In $[Os_{20}(CO)_{40}]^{2-}$ (**5**) the overall polyhedral disposition of the 40 terminal COs gives rise to different localized ligand environments about each of the three dissimilar kinds of metal atoms (Figure 3)—viz, three COs coordinated to each of the four corner Os(C) atoms, two COs linked to each of the 12 inner edge-bridging Os(B) atoms, and one CO coordinated to each of the four Os(A) atoms centered on the four 10-atom tetrahedral (111) faces.

In contrast to the resulting 40 ligand connectivities (viz, one for each terminal CO) in **5**, the particular distribution of 26 ligands about the $Pd_{16}Ni_4$ core in **1** (vide supra) produces 44 ligand connectivities (viz, one for each of the four PPh_3 and four terminal CO ligands, and two for each of the 18 doubly bridging COs). The ligand connectivities are the same for the face-centered four M(A) atoms and the edge-bridging 12 M(B) atoms; the four extra ligand connectivities in **1** result from a tetrahedral-like coordination of one terminal and three bridging CO ligands to each corner atom in **1** versus a trigonal pyramidal ligand coordination involving three terminal CO ligands to each corner atom in **5**. Both ligand arrangements, which preserve the pseudo T_d symmetry of the ν_3 tetrahedral metal-core geometry, have stereochemical implications with regard to the different possible modes of carbon monoxide attachment to close-packed (111) metal surfaces that depend on the ligand-to-metal (L/M) ratio. The 40 terminal COs in **1** are the maximum number that can be sterically accommodated on the Os_{20} surface. Hence, the terminal CO linkages found in $[Os_{20}(CO)_{40}]^{2-}$, for which the L/M ratio is 2.0, would possibly occur only for a saturated carbon monoxide coverage of small ccp metal crystallites. On the other hand, for a much smaller L/M ratio of 1.3 found in the ccp $Pd_{16}Ni_4$ cluster, it is presumed that the carbon monoxide coverage of small ccp metal crystallites would instead parallel the ligand-arrangement observed in **1** with doubly bridging carbonyl ligands along the ccp metal edges and with one terminal CO per corner metal atom. In both cases the face-centered metal atoms within the (111) metal terraces would each be expected from steric considerations to have a maximum of one attached terminal CO. This use of the different ligand-to-metal (L/M) linkages found in these two discrete metal clusters with isostructural ccp metal cores as model systems to describe the possible modes of carbon monoxide absorption on analogous metal surfaces appears to be consistent with some of the results (although controversial) deduced from extensive experimental/theoretical surface-science studies.[10, 44]

A comparison of the resulting relative variations in the metal-core means (Table 1) in $[Pd_{16}Ni_4(CO)_{22}(PPh_3)_4]^{2-}$ (**1**) with those in $[Os_{20}(CO)_{40}]^{2-}$ (**5**) dramatically illustrates the marked geometrical influence on the common metal framework due to the particular change from 40 terminal CO ligands in **5** to four terminal COs, 18 edge-bridging COs, and four PPh_3 ligands in **1**. In each cluster the mean for the six equivalent M(A)−M(A) distances in the central $M(A)_4$ tetrahedron, which has a terminal carbonyl ligand attached to each M(A) atom, is virtually identical to that found in the bulk metal (viz, 2.75 Å for ccp Pd; 2.68 Å for hcp Os).[45] In **1** the means for the six CO-bridged Pd(B)−Pd(B) and 12 CO-bridged Ni−Pd(B) edge-connectivities are 0.04 and 0.16 Å *shorter* than that of 2.75 Å for the six Pd(A)−Pd(A) connectivities in the central $Pd(A)_4$ tetrahedron, whereas in **5** the corresponding six nonbridged Os(B)−Os(B) and 12 nonbridged Os(B)−Os(C) edge-connectivities are 0.07 and 0.12 Å *longer* than that of 2.68 Å for the six Os(A)−Os(A) connectivities in the central $Os(A)_4$ tetrahedron. This opposite bond-length trend in mean distances between the 18 edge-connectivities in **1** and **5** relative to their corresponding means in the central $M(A)_4$ tetrahedron is attributed to the electronically induced bond-length shortening effects of the 18 edge-bridging COs in **1** that span all three pairs of the four atoms along each of the 6 tetrahedral Ni−Pd(B)−Pd(B)−Ni edges. Conversely, in **1** the mean of 2.82 Å for the 24 equivalent Pd(A)−Pd(B) nonedge connectivities in the four $Pd(A)_3Pd(B)_3$ octahedra is significantly longer than the Pd(A)−Pd(A) mean of 2.75 Å but markedly shorter than the mean of 2.93 Å for the 12 equivalent Pd(B)−Pd(B) nonedge connectivities in the four $Pd(B)_3$ triangles of the $Pd(A)_3Pd(B)_3$ octahedra that are each capped by a Ni atom. In direct contrast, in **5** the means of 2.76 and 2.78 Å for the corresponding 24 Os(A)−Os(B) and 12 nonedge Os(B)−Os(B) connectivities, respectively, are similar to the means of 2.75 and 2.80 Å for the Os(B)−Os(B) and Os(B)−Os(C) edge-connectivities, respectively. It is apparent that the much weaker metal−metal bonds[46−48] in **1** as well as the different ligand arrangements in **1** and **5** markedly influence the M−M bond-length connectivities in the same ccp tetrahedral metal-core framework.

Table 1. Mean Metal−Metal Connectivities under Pseudo-T_d ($\bar{4}3m$) Symmetry and Corresponding Individual Ranges in $[Pd_{16}Ni_4(CO)_{22}(PPh_3)_4]^{2-}$ (**1**) as $[PPh_4]^+$ Salt

metal−metal connectivities[a]	*N*[b]	mean (Å)	range (Å)
Pd(A)−Pd(A)	6	2.75	2.773(1)−2.740(1)
Pd(A)−Pd(B)	24	2.82	2.889(1)−2.774(1)
CO-br Pd(B)−Pd(B)	6	2.71	2.742(1)−2.671(1)
Ni-br Pd(B)−Pd(B)	12	2.93	2.957(1)−2.895(1)
Ni−Pd(B)	12	2.59	2.611(2)−2.570(2)
mean Pd−Pd	48	2.83	2.957(1)−2.671(1)
mean Pd−M (M = Pd, Ni)	60	2.78	2.957(1)−2.570(2)
Ni−P	4	2.182	2.197(4)−2.173(4)

[a] Atom-labeling for the metal core is given in Figure 1. [b] *N* denotes the number of symmetry-equivalent metal−metal and Ni−P connectivities under T_d symmetry.

$[Pd_{33}Ni_9(CO)_{41}(PPh_3)_6]^{4-}$ Tetraanion (2). (a) Structural/Bonding Features. The $Pd_{33}Ni_9$ core of **2** possesses crystal-

(43) Mingos, D. M. P.; Lin, Z. *Chem. Phys.* **1989**, *137*, 15 and references therein.

(44) (a) Su, X.; Cremer, P. S.; Shen, Y. R.; Somorjai, G. A. *J. Am. Chem. Soc.* **1997**, *119*, 3994 and references therein. (b) Wong, Y.-T.; Hoffmann, R. *J. Phys. Chem.* **1991**, *95*, 859 and references therein. (c) Hu, P.; King, D. A.; Lee, M.-H.; Payne, M. C. (d) Ramsier, R. D.; Lee, K.-W.; Yates, J. T., Jr. *Surf. Sci.* **1995**, *322*, 243 and references therein. (e) Xu, J.; Hendriken, P. N.; Yates, J. T., Jr. *Langmuir* **1994**, *10*, 3663 and references therein. (f) Locatelli, A.; Brena, B.; Lizzit, S.; Comelli, G.; Cautero, G.; Paolucci, G.; Rosei, R. *Phys. Chem Lett.* **1994**, *73*, 90. (g) Reutt-Robey, J. E.; Doren, D. J.; Chabal, Y.-J.; Christman, S. B. *J. Chem Phys.* **1990**, *93*, 9113.

(45) Donohue, J. *The Structure of the Elements*; John Wiley and Sons: NY, 1974; p 216.

(46) (a) Hughes, A. K.; Wade, K. *Coord. Chem. Rev.* **2000**, *197*, 199 and references therein. (b) Hughes, A. K.; Wade, K. In *Metal Clusters in Chemistry*; Braunstein, P., Oro, L. A., Raithby, P. R., Eds.; Wiley-VCH: New York, 1999; Vol. 2, p. 1073 and references therein.

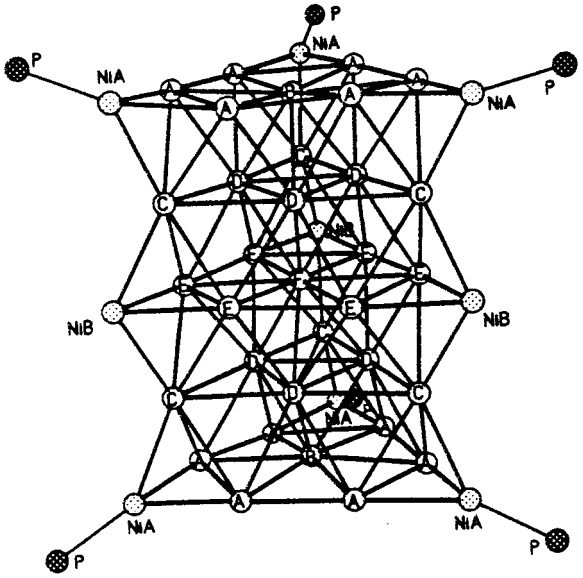

Figure 4. View of the 42-atom geometry of the $Pd_{33}Ni_9$ core in $[Pd_{33}Ni_9(CO)_{41}(PPh_3)_6]^{4-}$ (**2**). Its unique metal architecture of pseudo-D_{3h} hexagonal symmetry consists of five equilateral triangular layers that are stacked in a hcp [a(Pd_7Ni_3) b(Pd_6) a(Pd_7Ni_3) b(Pd_6) a(Pd_7Ni_3)] sequence. The one interior Pd(i) atom in the middle Pd_7Ni_3 layer has a localized hcp environment. Under pseudo-D_{3h} symmetry the $Pd_{33}Ni_9$ core has five different types of palladium atoms and two different types of nickel atoms.

lographic C_2-2 site symmetry and pseudo- $D_{3h}(\bar{6}2m)$ symmetry. Its 42-atom metal framework (Figure 4) consists of five approximately planar equilateral triangular layers that are stacked in a hcp arrangement. The identical top, middle, and bottom layers are each composed of a 10-atom ν_3 Pd_7Ni_3 triangle with the three Ni atoms at the corners and with the central interior Pd atom surrounded by a hexagon of palladium atoms. The identical symmetry-related second and fourth layers are each comprised of a ν_2 Pd_6 triangle. The central interior Pd(i) atom in the middle layer of this cluster is encapsulated by 12 hcp surface Pd(s) atoms. The crystallographic 2-fold axis corresponds to one of the three horizontal pseudo-2-fold axes within the middle Pd_7Ni_3 layer that passes through the interior Pd(i) atom, a corner Ni atom, and its attached terminal CO ligand; hence, one-half the cluster is crystallographically independent.

(47) The cohesive energy of the bulk metal is estimated by the standard enthalpy of atomization of the gaseous metal atom, ΔH_f^o [M(g)], being 791 kJ/mol for osmium versus 378 kJ/mol for palladium.[46] If the cohesive energy of the metal is assumed to originate in the metallic bonding between adjacent metal atoms in the lattice, it follows that each metal−metal bond contributes 2 ΔH_f^o [M(g)]/n kJ/mol, where n denotes the coordination number of each metal atom in the bulk metal. Because $n = 12$ for both hcp osmium metal and ccp palladium metal, the calculated mean metal−metal bond enthalpy, E(M−M), is 132 kJ/mol for osmium and 62 kJ/mol for palladium.[46]

(48) Of particular relevance are the recent bond length/bond enthalpy patterns recently put forth by Hughes and Wade[46] for osmium (and other homometallic) carbonyl clusters including $[Os_{20}(CO)_{40}]^{2-}$ (**5**). Their approach provides an estimation of the overall strength (i.e., total enthalpy) of the Os−Os bonds from the numbers of electrons supplied by the carbonyl ligands and anionic charges. Their model shows that less metal−metal bonding is possible with an increase in COs per osmium atom within a given cluster. The observed variations in the mean Os(C)−Os(B), Os(B)−Os(B), Os(B)−Os(A), and Os(A)−Os(A) distances of 2.80, 2.75, 2.76, and 2.68 Å, respectively, for the $(CO)_3$Os(C), $(CO)_2$Os(B), and (CO)Os(A) fragments in $[Os_{20}(CO)_{40}]^{2-}$ (**5**) are consistent with their results. Noteworthy is that their model also shows that metal−carbonyl bond enthalpies are much stronger than metal−metal bond enthalpies; that is, metal−metal bond cleavage accounts for only a small percentage (less than 20%) of the total disruption enthalpy of gaseous $M_x(CO)_y$ (g) into x M (g) and y CO (g).

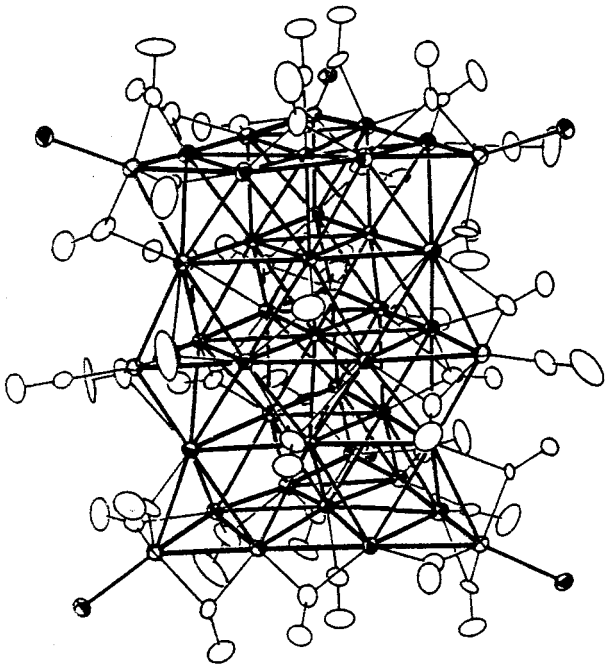

Figure 5. Configuration of $[Pd_{33}Ni_9(CO)_{41}(PPh_3)_6]^{4-}$ (**2**) without the phosphorus-attached phenyl substituents. Its close-packed 42-atom metal-core geometry containing 12 octahedral and 28 tetrahedral holes is encapsulated by six Ni-attached triphenyl phosphine ligands, three Ni-attached and two Pd-attached terminal COs, and 24 edge-bridging and 12 face-bridging COs; the connectivities of six face-bridging COs violate the pseudo horizontal mirror plane and reduce the pseudo-D_{3h} symmetry of the $Pd_{33}Ni_9$ core to D_3 for the tetraanion (excluding the phenyl substituents). **2** possesses a crystallographic C_2 axis which corresponds to one of the three horizontal pseudo-2-fold axes (within the middle Pd_7Ni_3 layer) that pass through the interior Pd(i) atom, a corner Ni atom, and its attached terminal carbonyl ligands; hence, one-half of this cluster anion is crystallographically independent.

The resulting pseudo-D_{3h} hcp $Pd_{33}Ni_9$ core has 12 octahedral and 28 tetrahedral holes.

Figure 5 presents a view of the entire $[Pd_{33}Ni_9(CO)_{41}(PPh_3)_6]^{4-}$ tetraanion (excluding the phenyl substituents). The six triphenyl phosphine ligands are attached to the six corner nickel atoms in the top and bottom layers. The 41 carbonyl groups consist of five terminal and 36 bridging ligands. The terminal COs are coordinated to the three corner Ni atoms in the middle layer and to the two central Pd atoms in the top and bottom layers. Of the 36 bridging COs, 24 are edge-bridging and the other 12 are face-bridging. Eighteen of the edge-bridging COs span the 12 Ni−Pd and 6 Pd−Pd edge-connectivities within the symmetry-equivalent top and bottom Pd_7Ni_3 layers; the other six edge-bridging COs link the six Ni(corner)−Pd(corner) edges between the top two and bottom two Pd_7Ni_3 and Pd_6 layers. Each of these six nickel atoms in the top and bottom layers has a localized tetrahedral-like ligand environment made up of its terminal PPh_3 ligand and three edge-bridging COs. The 12 face-bridging COs connect the middle Pd_7Ni_3 layer with the two adjacent (second/fourth) Pd_6 layers. Six COs cap each of the six triangular Pd_3 faces formed from the two adjacent internal Pd atoms of the three edges in the middle layer with the single internal-edge Pd atoms in both the second and fourth Pd_6 layers; the other six COs each cap in an alternating sequence only six of the 12 triangular $NiPd_2$ faces formed from the six Pd−Ni edge-connectivities in the middle Pd_7Ni_3 layer with the corner Pd atoms in the second and fourth Pd_6 layers. The resulting localized ligand coordination of the terminal and two triply bridging COs about each corner nickel atom in the middle layer is approximately trigonal planar. Although the overall disposition

Table 2. Mean Metal−Metal Connectivities under Pseudo-D_{3h} Symmetry and Corresponding Individual Ranges in $[Pd_{33}Ni_9(CO)_{41}(PPh_3)_6]^{4-}$ (**2**) as $[PPh_4]^+$ Salt

metal−metal connectivities[a]	N[b]	mean (Å)	range (Å)
CO-br Pd(A)−Pd(A)	6	2.71	2.725(2)−2.694(2)
Ni-br Pd(A)−Pd(A)	6	2.93	2.957(2)−2.906(2)
Pd(A)−Pd(B)	12	2.82	2.886(2)−2.765(2)
Pd(A)−Pd(C)	12	2.88	2.907(2)−2.838(2)
Pd(A)−Pd(D)	12	2.85	2.927(2)−2.785(2)
Pd(B)−Pd(D)	6	2.72	2.736(2)−2.711(2)
Pd(C)−Pd(D)	12	2.87	2.929(2)−2.811(2)
Pd(C)−Pd(E)	12	2.86	3.024(2)−2.735(2)
Pd(D)−Pd(D)	6	2.83	2.835(2)−2.824(2)
Pd(D)−Pd(E)	12	2.78	2.821(2)−2.746(2)
Pd(D)−Pd(F)	6	2.78	2.820(2)−2.778(2)
CO-br Pd(E)−Pd(E)	3	2.78	2.781(2)−2.773(2)
Ni-br Pd(E)−Pd(E)	3	2.81	2.811(2)−2.794(2)
Pd(E)−Pd(F)	6	2.79	2.792(2)−2.790(2)
mean Pd−Pd	114	2.82	3.024(2)−2.694(2)
Ni(A)−Pd(A)	12	2.58	2.632(2)−2.556(2)
Ni(A)−Pd(C)	6	2.67	2.687(2)−2.643(2)
Ni(B)−Pd(C)	6	2.69	2.710(2)−2.674(2)
Ni(B)−Pd(E)	6	2.63	2.649(2)−2.625(2)
Mean Pd−Ni	30	2.64	2.710(2)−2.555(2)
Ni(A)−P	6	2.19	2.194(5)−2.182(5)

[a] Atom-labeling for the metal core is given in Figure 4. [b] N denotes the number of symmetry-equivalent metal−metal and Ni−P connectivities under D_{3h} symmetry.

of the 36 bridging carbonyls about the $Pd_{33}Ni_9$ framework varies widely from pseudo-3-fold symmetry due to steric effects (i.e., as evidenced by zigzag arrangements of adjacent COs along the polyhedral metal−metal edges), only the ligand−metal connectivities of these latter six face-bridging COs violate the pseudohorizontal mirror plane and thereby reduce the pseudo-D_{3h} symmetry of the $Pd_{33}Ni_9$ core to D_3 for the tetraanion (excluding the phosphorus-attached phenyl substituents).

Figure 4 shows that under D_{3h} symmetry the $Pd_{33}Ni_9$ core in **1** has five different types of palladium atoms and two different types of nickel atoms. Table 2 reveals that the 114 individual Pd−Pd and 30 individual Pd−Ni bonding distances are distributed among 14 different kinds of Pd−Pd and four different kinds of Pd−Ni connectivities, respectively. Considerable differences are observed among the 14 different Pd−Pd means; the shortest and longest means of 2.705 and 2.93 Å are found within the top and bottom Pd_7Ni_3 layers for the six CO(edge)-bridged and six Ph_3PNi-bridged Pd−Pd′ tangential connectivities, respectively. The overall mean of 2.82 Å for the 114 Pd−Pd distances is 0.07 Å longer than that of 2.75 Å in ccp Pd metal. Likewise, of the four means of 2.58, 2.63, 2.67, and 2.69 Å for the four different kinds of Pd−Ni connectivities which are all spanned by doubly or triply bridging COs, the smallest mean is also found within the top and bottom Pd_7Ni_3 layers for the 12 CO-(edge)-bridged Pd−Ni tangential connectivities. It is apparent that the different bonding modes of the 36 bridging carbonyl ligands play an important role in influencing the metal−metal distances. In contrast, the six individual Ni−P distances (of which three are crystallographically independent) deviate by less than 0.01 Å from the mean of 2.19 Å.

The six terminal PPh_3 and five terminal, 24 doubly bridging, and 12 triply bridging COs combine to form 95 links with the $Pd_{33}Ni_9$ core. This ligand arrangement gives rise to a markedly nonequivalent distribution to the 41 surface metal atoms—viz, one CO connected to each of the two Pd(B) and six Pd(D) atoms, two COs connected to each of the 12 Pd(A) and 6 Pd(C) atoms, three COs connected to each of the three Ni(B) and six Pd(E) atoms, and one PPh_3 and three COs connected to each of the six Ni(A) atoms. Based upon a detailed examination of the bonding nature of the ligands and their distances from each type of metal atom coupled with the number of nearest metal neighbors, we conclude that each of the 41 metal surface atoms has an approximately equivalent charge density.

The observed number of metal cluster valence electrons (CVEs) in this hcp cluster, which has globally delocalized metal−metal bonding, is 518 electrons (i.e., 33 × 10 (Pd) + 9 × 10 (Ni) + 41 × 2 (CO) + 6 × 2 (PPh_3) + 4 (charge) = 518). This number is in exact agreement with the predicted number of CVEs obtained from the Lauher/Ciani-Sironi model,[34,36] the Mingos model,[37,38] and the Teo-Zhang model,[39,40] for high-nuclearity closed-packed metal clusters.

Comparative Structural/Bonding Analysis of $[Pd_{16}Ni_4(CO)_{22}(PPh_3)_4]^{2-}$ (1) and $[Pd_{33}Ni_9(CO)_{41}(PPh_3)_6]^{4-}$ (2) and Resulting Implications. Both **1** and **2** are two rare examples of a palladium carbonyl cluster that has terminal carbonyl ligands.[49−55] As stated earlier, palladium is the only late transition metal (Groups 8−10) that does not form stable discrete binary homometallic metal carbonyl clusters at room temperature. This may be partly ascribed to palladium metal having the weakest metal−metal bonds (i.e., those with the smallest cohesive energy) of all the metals in the iron, cobalt, and nickel triads, as estimated by its significantly lower standard enthalpy of atomization of the gaseous metal atom.[46,47] The nonisolation (to date) of binary palladium carbonyl clusters at room temperature may be attributed not only to weak Pd−Pd bonding but also to weak Pd−CO(terminal) bonding.[56] The existence of **1** and **2** with a terminal CO (instead of a PPh_3) coordinated to the centered Pd(A) atom on each of the four tetrahedral $Pd(A)Pd(B)_6Ni_3$ faces in **1** and to the centered Pd(B) atom on

(49) In complete opposition to countless nickel complexes containing terminal carbonyl ligands, only a relatively few palladium complexes containing terminal carbonyl ligands are known,[50] of which a considerable number are thermally unstable. The highest terminal carbonyl frequency for the handful of mononuclear ones,[50a,b] and for the bent bis-(square planar) $Pd_2(\mu_2\text{-}Cl)_2(CO)_4$ dimer[50c] is above 2050 cm^{-1} thereby indicating weak Pd−CO bonding interactions. Lower carbonyl frequencies observed for the terminal carbonyls in the crystallographically determined triangular $Pd_3(\mu_2\text{-}t\text{-}Bu_2P)_3(CO)_2Cl$ (hexane: 2035, 2030 cm^{-1})[50d] and $Pd_3(\mu_2\text{-}Sn(N(SiMe_3)_2)_3(CO)_3$ (Nujol: 2038 cm^{-1})[50e] are presumed to be a consequence of strong electron donation by the bridging ligands, resulting in a sufficiently high negative partial charge on the palladium atoms to promote significant Pd−CO π-back-bonding.

(50) (a) Whyman, *J. Organomet. Chem.* **1973**, *63*, 467. (b) Jones, P. G. *Z. Naturforsch.* **1982**, *37b*, 823 and references therein. (c) Soriano-Garcia, M.; Rosas, N.; Gomez-Lara, J.; Toscano, R. A. *Acta Crystallogr.* **1987**, *C43*, 1679. (d) Arif, A. M.; Heaton, D. E.; Jones, R. A.; Nunn, C. M. *Inorg. Chem.* **1987**, *26*, 4228. (e) Campbell, G. K.; Hitchcock, P. B.; Lappert, M. F.; Misra, M. C. *J. Organomet. Chem.* **1985**, *289*, C1.

(51) See footnotes 29 and 30 in ref 2d.

(52) Only two other geometrically analogous and electronically equivalent palladium carbonyl phosphine clusters possess terminal COs: namely, $Pd_{10}(CO)_2(\mu_2\text{-}CO)_8(\mu_3\text{-}CO)_4(PBu^n_3)_4$ (**7**)[53] and $Pd_{10}(CO)(\mu_2\text{-}CO)_8(\mu_3\text{-}CO)_4(PPr^i_3)_5$.[54] These two clusters may be considered as carbonyl derivatives of $Pd_{10}(\mu_2\text{-}CO)_8(\mu_3\text{-}CO)_4(PBu^n_3)_6$ (**6**)[55] in that each has a similar tetra-Pd-capped Pd_6 octahedron of pseudotetragonal D_{2d} (42m) symmetry (without the P-attached substituents). Compound **7** is transformed into **6** by the substitution of two terminal COs in place of the two PBu^n_3 ligands coordinated to the two apical Pd(ap) atoms of the Pd_6 octahedron. The "hybrid" derivative, $Pd_{10}(CO)(\mu_2\text{-}CO)_8(\mu_3\text{-}CO)_4(PPr^i_3)_5$, has a terminal CO coordinated to one Pd(ap) atom and a phosphine ligand to the other Pd(ap) atom of the Pd_6 octahedron.

(53) Mednikov, E. G.; Eremenko. N. K.; Slovokhotov, Yu. L.; Struchkov, Yu. T.; Gubin, S. P. *J. Organomet. Chem.* **1983**, *258*, 247.

(54) Wittayakun, J.; Tran, N. T.; Powell, D. R.; Dahl, L. F. Manuscript in preparation.

(55) Mednikov, E. G.; Eremenko. N. K.; Gubin, S. P.; Slovokhotov, Yu. L.; Struchkov, Yu. T. *J. Organomet. Chem.* **1982**, *239*, 401.

(56) (a) Chung, S.-C.; Krüger S.; Ruzankin, S. P.; Pacchioni, G.; Rösch, N. *Chem. Phys. Lett.* **1996**, *248*, 109. (b) Chung, S.-C.; Krüger S.; Pacchioni, G.; Rösch, N. *J. Chem. Phys.* **1995**, *102*, 3695.

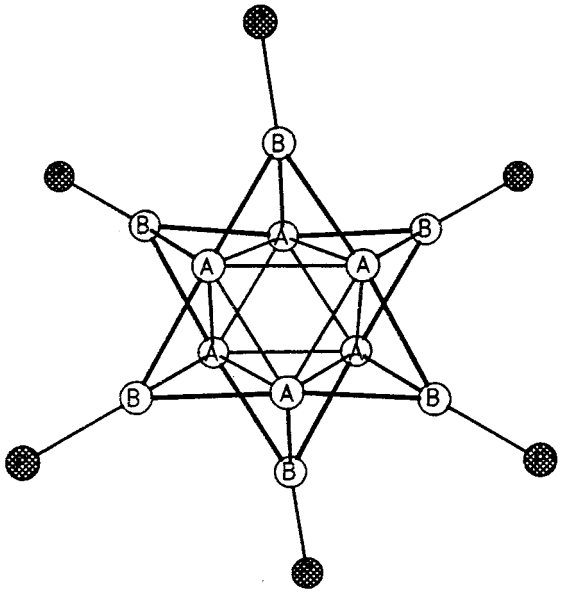

Figure 6. View of the close-packed Pd_{12} core-geometry in $Pd_{12}(\mu_2\text{-}CO)_6(\mu_3\text{-}CO)_6(PPh_3)_6$ (**3**). Its metal architecture of pseudo-D_{3d} symmetry may be envisioned as a highly deformed octahedral Pd_6 kernel which is capped on six of its eight triangular faces by Pd atoms.

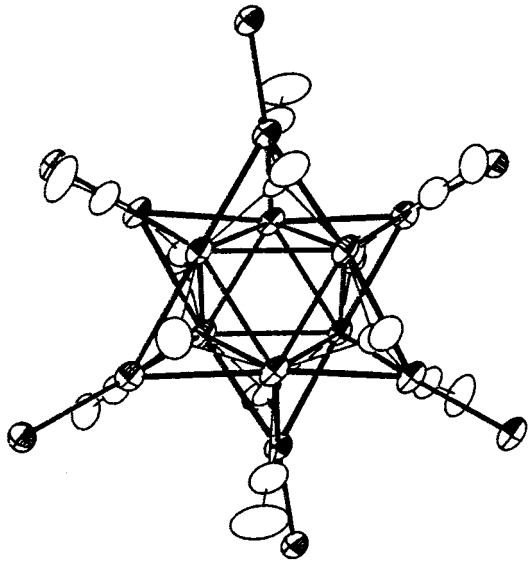

Figure 7. Molecular geometry of neutral $Pd_{12}(\mu_2\text{-}CO)_6(\mu_3\text{-}CO)_6(PPh_3)_6$ (**3**) showing the distribution of the 18 ligands (without the phosphorus-attached phenyl rings) about the Pd_{12} core of pseudo-D_{3d} symmetry. Six PPh_3 ligands are each terminally coordinated to one of the six capping Pd atoms. Of the 12 bridging COs that lie on the three pseudo σ_d vertical mirror planes, each of the six edge-bridging COs links one of the six capping Pd atoms to the adjacent kernel Pd atom lying on the same mirror plane. The capping Pd atom is also connected via one of the six face-bridging COs with the two mirror-related kernel Pd atoms that form a triangular face with the capping Pd atom.

each of the analogous two outer faces in **2** is undoubtedly a consequence of steric effects.

Palladium and nickel metals per se have been shown from a variety of experimental measurements[22] to form a continuous series of solid solutions at room temperature. Nevertheless, our crystallographic results revealed that these two carbonyl-ligated Pd−Ni clusters attain an ordered metal-atom core without site substitutional disorders. This observed site ordering of the metal-core atoms in these two Pd−Ni clusters must be a ligand-induced effect arising from the markedly different coordination behavior between Ni and Pd atoms for carbonyl ligands.

$Pd_{12}(\mu_2\text{-}CO)_6(\mu_3\text{-}CO)_6(PPh_3)_6$ (3). (a) Structural/Bonding Features. The Pd_{12} core of **3** (Figure 6) may be best described as two ν_2 $Pd(A)_3Pd(B)_3$ triangles, each containing three Pd(B)−Pd(A)−Pd(B) bonding edges with an inner bonding $Pd(A)_3$ triangle. These two symmetry-identical triangular layers are centrosymmetrically oriented in a staggered stacked close-packed array such that the *intralayer*-bonding inner $Pd(A)_3$ triangles form a regular trigonal antiprism. The resulting Pd_{12} core-geometry closely conforms to trigonal D_{3d} ($\bar{3}2/m$) symmetry with the principal 3-fold axis passing through the midpoints of the two $Pd(A)_3$ triangles. Figure 6 shows that each of the six symmetry-equivalent Pd(A) atoms caps the two *interlayer* Pd(A) atoms and their adjacent edge-bridged Pd(B) atom which corresponds to the close-packed Pd_{12} core possessing one octahedral and six tetrahedral holes. Alternatively, the Pd_{12} framework in **3** may be described as a highly deformed central octahedral $Pd(A)_6$ kernel which is capped on six of its eight triangular faces by Pd(B) atoms.

Addition of the PPh_3 and CO ligands to the Pd_{12} core (Figure 7) preserves the centrosymmetric pseudo-D_{3d} symmetry (without the P-attached phenyl substituents). The six PPh_3 ligands are each coordinated to one of the six Pd(B) atoms. The 12 carbonyl ligands consist of six doubly bridging and six triply bridging COs, each of which lies on one of the three σ_d vertical mirror planes. Each of the six doubly bridging COs edge-bridges one of the six Pd(B) atoms and the adjacent kernel Pd(A) atom lying on the same vertical mirror plane. Likewise, one of the six triply bridging COs is connected to this Pd(B) atom on the same vertical mirror plane and the two mirror-related kernel Pd(A) atoms that form a triangular face with the capping Pd atom.

Of particular interest is that the average molecular parameters (Table 3) for **3** reveal that the geometry of the inner Pd_6 kernel is greatly distorted from a regular octahedron. This trigonal antiprismatic D_{3d} deformation is evidenced primarily by the six *intralayer* Pd(A)−Pd(A) edges having a mean of 2.77 Å (which corresponds to that of 2.75 Å in ccp Pd metal) versus the six *interlayer* Pd(A)−Pd(A) edges having a 0.4 Å longer mean of 3.17 Å which may be considered as nonbonding or at most weakly bonding.

On the other hand, the 12 *intralayer* and six *interlayer* Pd(A)−Pd(B) means of 2.82 and 2.72 Å, respectively, are within the normal Pd−Pd bonding range; the 0.1 Å shorter *interlayer* Pd(A)−Pd(B) mean is attributed to these bonding connectivities being spanned by the six edge-bridged carbonyl ligands. Consequently, the two triangular $Pd(A)_3Pd(B)_3$ layers are essentially linked to each other only by the six *interlayer* CO-bridged Pd(A)−Pd(B) connectivities.

The isostructural $Pd_{12}(CO)_{12}(PBu^n_3)_6$ (**6**) was recently reported by Mednikov et al.[57] from both the reaction involving the mild oxidation of mixed $Pd_{10}(CO)_{12}(PBu^n_3)_6/Pd_4(CO)_5(PBu^n_3)_4$ clusters with Me_3NO (in HOAc) and the reaction of $Pd_{10}(CO)_{12}(PBu^n_3)_6$ with $Pd_2(dba)_3$ (where dba denotes dibenzylideneacetone). Table 3 shows that the overall geometry of this tri-*n*-butyl phosphine cluster (**6**) is virtually identical to that of **3** with the corresponding means for the two Pd_{12} cores differing by <0.02 Å, except for the weakly bonding (or nonbonding) *interlayer* Pd(A)−Pd(A) means which differ by 0.06 Å.

(b) Structural/Bonding Comparison of $Pd_{12}(\mu_2\text{-}CO)_6(\mu_3\text{-}CO)_6(PR_3)_6$ (R═Ph (3), n-Bu (6)) with Related Homopalladium and Heteropalladium Clusters and Resulting Impli-

(57) Mednikov, E. G.; Struchkov, Yu. T.; Slovokhotov, Yu. L. *J. Organomet. Chem.* **1998**, *566*, 15.

Table 3. Comparison of Corresponding Means under Pseudo-D_{3d} ($\bar{3}2/m$) Symmetry in the Isostructured $Pd_{12}(\mu_2\text{-}CO)_6(\mu_3\text{-}CO)_6(PR_3)_6$ (R = Ph (**3**), *n*-Bu (**6**)) and Geometrically Related $[Pd_6Ru_6(CO)_{24}]^{2-}$ ($[NEt_4]^+$ Salt) and $[HPd_6Fe_6(CO)_{24}]^{3-}$ ($[N(CH_2Ph)Me_3]^+$ Salt)

metal−metal connectivities[a]	N[b]	mean (Å)	range (Å)	mean (Å)	range (Å)
		$Pd_{12}(CO)_{12}(PPh_3)_6$ (**3**)[c]		$Pd_{12}(CO)_{12}(PBu^n_3)_6$ (**6**)[d]	
intralayer Pd(A)−Pd(A)	6	2.77	2.820(1)−2.744(1)	2.75	2.759(4)−2.740(4)
intralayer Pd(A)−Pd(B)	12	2.82	2.868(1)−2.798(1)	2.81	2.812(4)−2.792(4)
interlayer Pd(A)−Pd(A)	6	3.17	3.372(1)−3.027(1)	3.23	3.365(4)−3.119(4)
interlayer Pd(A)−Pd(B)	6	2.72	2.730(1)−2.711(1)	2.70	2.702(4)−2.691(4)
		$[Pd_6Ru_6(CO)_{24}]^{2-}$ (M(B) = Ru)[e]		$[Fe_6Pd_6(CO)_{24}H]^{2-}$ (M(B) = Fe)[f,g]	
intralayer Pd(A)−Pd(A)	6	2.78	2.798(1)−2.767(2)	2.81	
intralayer Pd(A)−M(B)	12	2.79	2.804(1)−2.785(1)	2.70	
interlayer Pd(A)−Pd(A)	6	3.18	3.274(2)−3.068(1)	2.95	
interlayer Pd(A)−M(B)	6	2.68	2.685(1)−2.680(1)	2.61	

[a] Atom-labeling for the metal core is given in Figure 6. [b] *N* denotes the number of symmetry-equivalent metal−metal connectivities under D_{3d} symmetry. [c] This work. [d] Ref 57. [e] Ref 25. [f] Ref 24, 25. [g] Individual distances were not given.

cations. Table 3 reveals that the homometallic Pd_{12} framework in **3** (Figure 6) and **6** is geometrically related to the heterometallic Pd_6M_6 frameworks (M = Fe, Ru) of hexa-M-capped octahedral Pd_6 kernels found in the isostructural but electronically nonequivalent $[HPd_6Fe_6(CO)_{24}]^{3-}$ trianion[24,25] and $[Pd_6Ru_6(CO)_{24}]^{2-}$ dianion.[25] The corresponding *intralayer* Pd(A)−Pd(A) mean distances in the Pd_6Fe_6 and Pd_6Ru_6 clusters are 2.81 and 2.78 Å, respectively, while the *interlayer* Pd(A)−Pd(A) mean distances are 2.95 and 3.18 Å, respectively. The significantly longer *interlayer* connectivities likewise point to a large geometrical distortion of the $Pd(A)_6$ kernel in the Pd_6Fe_6 and Pd_6Ru_6 clusters from a regular octahedron toward a trigonal antiprism. The corresponding *intralayer* Pd(A)−M mean distances of 2.70 Å (M = Fe) and 2.79 Å (M = Ru) and *interlayer* Pd(A)−M distances of 2.61 Å (M = Fe) and 2.68 Å (M = Ru) are also consistent with metal−metal bonding interactions being comparable to those in **3** and **6**. Of interest is that Mednikov et al.[57] pointed out that the aforementioned nonbonding *interlayer* Pd(A)−Pd(A) connectivities in the $Pd(A)_6$ trigonal antiprism of **6** suggest that its Pd_{12} polyhedron may be an intermediate geometry type between a regular hexacapped octahedron stretched along its 3-fold axis and a noncentered icosahedron compressed along the same axis.

The observed number of CVEs for **3** and **6** is 156 (i.e., 12 × 10(Pd) + 12 × 2(CO) + 6 × 2(PPh_3) = 156). This electron count is two less than that of 158 electrons obtained via each of the Lauher/Ciani-Sironi, Mingos, and Teo/Zhang models.[36,38,40] If **3** and **6** are considered instead as a hexacapped Pd_6 octahedron, the observed electron count is 84 CVEs versus the predicted value of 86 CVEs for a capped metal octahedron. The corresponding observed electron counts for the hexacapped Pd_6 octahedra in $[HPd_6Fe_6(CO)_{24}]^{3-}$ and $[Pd_6Fe_6(CO)_{24}]^{2-}$ are 88 and 86 electrons, respectively.

A subsequent examination revealed a similar deficiency in observed versus predicted electron counts for other palladium and platinum carbonyl phosphine clusters. For example, both $Pd_6(\mu_3\text{-}CO)_4(PMe_3)_7$,[58] which has a distorted octahedral Pd_6 core of pseudo-C_{2v} symmetry with face-capping COs on alternate triangular faces and seven terminal PMe_3 ligands, and $[Pt_6(CO)_6(\mu_2\text{-}dppm)_3]^{2+}$ (as the $[BPh_4]^-$ salt),[59] which has a deformed octahedral Pt_6 core, have only 82 observed CVEs instead of the predicted 86. In sharp contrast, 86-electron configurations are observed for the octahedral metal cores of the neighbor Ni and Rh elements in the $[Ni_6(CO)_{12}]^{2-}$ dianion,[60] $Rh_6(CO)_{16}$,[61] $Rh_6(CO)_{12}(P(OPh)_3)_4$,[62] and $Rh_6(CO)_{10}(dppm)_3$.[63]

Several other structurally determined clusters possessing Pd-capped Pd_6 octahedra have notable metal topologies and electronic configurations of special relevance to those of **3** and **6**. Whereas both the monocapped Pd_6 octahedron in $Pd_7(\mu_2\text{-}CO)_3(\mu_3\text{-}CO)_4(PMe_3)_7$[64] and the bicapped Pd_6 octahedron in $Pd_8(\mu_2\text{-}CO)_6(\mu_3\text{-}CO)_2(PMe_3)_7$[65] conform to the 86-electron configuration, the tetracapped Pd_6 octahedra in the electronically equivalent $Pd_{10}(\mu_2\text{-}CO)_8(\mu_3\text{-}CO)_4(PBu^n_3)_6$ (**7**)[55] and $Pd_{10}(CO)_2(\mu_2\text{-}CO)_8(\mu_3\text{-}CO)_4(PBu^n_3)_4$ (**8**)[53] possess 88-electron configurations. King[66] proposed a qualitative delocalized valence bond model for **7** and **8** which reconciles the two additional electrons in electron counting.

In all of these clusters the face-capping of the Pd_6 octahedra is similarly unsymmetrical in that one of the three connectivities between each capping Pd(cap) atom and the three Pd(oct) atoms of the triangular face being capped is much longer (3.1−3.4 Å) than the other two connectivities (2.69−2.73 Å). However, King[66] pointed out that this difference of a "closed" versus an "open" cap does *not* affect the electron counting of the central polyhedron (i.e., in this case the octahedron). These "open" cap clusters were attributed by Goddard et al.[64] for the monocapped Pd_6 octahedron in the Pd_7 cluster and by Mednikov et al.[55] for the tetracapped Pd_6 octahedra in the two Pd_{10} clusters to the occupation of a low-lying antibonding MO. In the limiting case this "open" cap corresponds to a 16-electron trigonal planar Pd(cap) atom. The deficiency of the CV MOs in these palladium clusters has been ascribed to the shifting of one or two of the valence p AOs to such high energies in the late transition metals (particularly Pd and Pt) that they no longer participate significantly in the bonding.

Mednikov et al.[53] found that $Pd_{10}(CO)_2(\mu_2\text{-}CO)_8(\mu_3\text{-}CO)_4(PBu^n_3)_4$ (**8**) is considerably more unstable than $Pd_{10}(\mu_2\text{-}CO)_8(\mu_3\text{-}CO)_4(PBu^n_3)_6$ (**7**) and that the corresponding triethyl phosphine analogues of **7** and **8** are much less stable such that the triethyl phosphine analogue of **8** cannot be isolated in pure form. On this basis they suggested that the incorporation of bulky substituted phosphines should increase the stability due to the more effective shielding of its surface, given the same number

(58) Klein, H.-F.; Mager, M.; Flörke, U.; Haupt, H.-J. *Organometallics* **1992**, *11*, 3915.
(59) Hao, L.; Spivak, G. J.; Xiao, J.; Vittal, J. J.; Puddephatt, R. J. *J. Am. Chem. Soc.* **1995**, *117*, 7011.
(60) Calabrese, J. C.; Dahl, L. F.; Cavalieri, A.; Chini, P.; Longoni, G.; Martinengo, S. *J. Am. Chem. Soc.* **1974**, *96*, 2616.
(61) Corey, E. R.; Dahl, L. F.; Beck, W. *J. Am. Chem. Soc.* **1963**, *85*, 1202.
(62) Ciani, G.; Manassero, M.; Albano, V. G. *J. Chem. Soc., Dalton Trans.* **1981**, 515.
(63) Ceriotti, A.; Ciani, G.; Garlaschelli, L.; Sartorelli, U.; Sironi, A. *J. Organomet. Chem.* **1982**, *229*, C9.
(64) Goddard, R.; Jolly, P. W.; Krüger, C.; Schick, K.-P.; Wilke, G. *Organometallics* **1982**, *1*, 1709.
(65) Bochmann, M.; Hawkins, I.; Hursthouse, M. B.; Short, R. L. *Polyhedron* **1987**, *6*, 1987.
(66) King, R. B. *Gazz. Chim. Ital.* **1992**, *122*, 383.

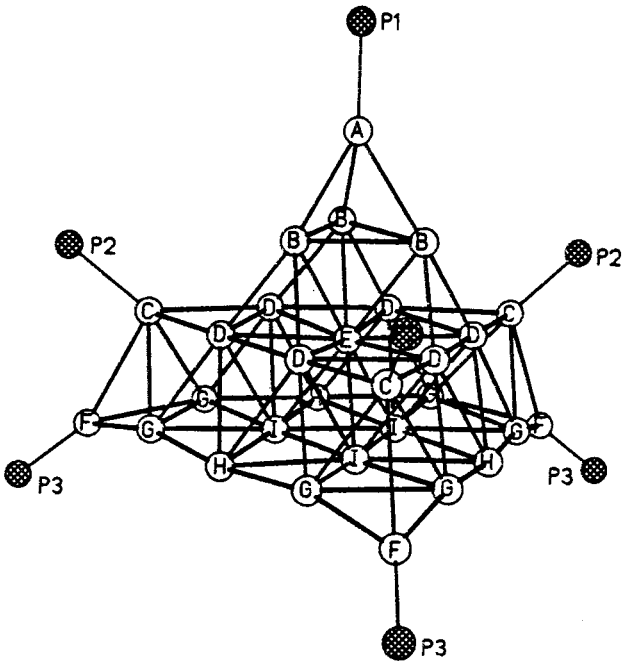

Figure 8. View of the close-packed Pd_{29} core-geometry in $[Pd_{29}(\mu_2\text{-}CO)_{15}(\mu_3\text{-}CO)_{13}(PPh_3)_7]^{2-}$ (**4**). Its unprecedented nonconvex metal polyhedron of pseudo C_{3v} trigonal symmetry may be described as a four-layer stacking along the 3-fold principal axis of 29 atoms in a mixed hcp/ccp [a(Pd_1) b(Pd_3) a(Pd_{10}) c(Pd_{15})] sequence; the one interior Pd(i) atom in the third layer has a localized ccp environment. Under pseudo-C_{3v} symmetry the Pd_{29} core has nine different types of palladium atoms.

of ligands in the coordination sphere of a metal polyhedron. Likewise, the fact that PMe_3 and PEt_3 analogues of **3** and **6** have not been isolated[2c,57] indicates that bulky phosphine ligands are also necessary in order to stabilize $Pd_{12}(\mu_2\text{-}CO)_6(\mu_3\text{-}CO)_6(PR_3)_6$ clusters. This compelling evidence emphasizing the influence of bulky phosphine substituents in stabilizing particular types of palladium carbonyl phosphine clusters coupled with the relatively few known palladium carbonyl clusters with terminal carbonyl ligands (vide supra) indicates that the oligomeric nature of the palladium cores and concomitant compositions of this important class of palladium clusters are synergically dictated by combined steric/electronic ligand effects.

$[Pd_{29}(\mu_2\text{-}CO)_{15}(\mu_3\text{-}CO)_{13}(PPh_3)_7]^{2-}$ (4): Structural/Bonding Features. This dianion (as the $[PPh_4]^+$ salt) possesses a geometrically unprecedented close-packed Pd_{29} core (Figure 8), which may be described as a four-layer stacking of 29 atoms in a mixed hcp/ccp [a(Pd_1) b(Pd_3) a(Pd_{10}) c(Pd_{15})] sequence. This nonconvex metal polyhedron of pseudo trigonal C_{3v} (3*m*) symmetry has one interior and 28 surface atoms. The interior Pd(i) in the third layer has a localized ccp environment corresponding to a centered cuboctahedron. Table 4 presents the mean metal−metal distances in the Pd_{29} core under C_{3v} symmetry; the mean of 2.82 Å for the 87 individual Pd−Pd distances is 0.07 Å longer than that for ccp palladium metal.

The arrangement of the seven triphenyl phosphine phosphorus and 28 bridging carbonyl ligands about the four-layer Pd_{29} core preserves the pseudo C_{3v} symmetry (Figure 9). The seven terminal PPh_3 ligands are coordinated to the top-layer apical Pd(ap) atom and to the three corner atoms in the third and fourth triangular layers. Three edge-bridged COs link the Pd(ap) atom to the three triangular Pd atoms in the second layer. In turn, three triply bridging interlayer COs each cap one of these triangular Pd atoms in the second layer and two interior Pd atoms along one of the three 4-atom triangular edges of the

Table 4. Mean Metal−Metal Connectivities under Pseudo-C_{3v} (3m) Symmetry and Corresponding Individual Ranges in $[Pd_{29}(Co)_{28}(PPh_3)_7]^{2-}$ (**4**) as $[PPh_4]^+$ Salt

metal−metal connectivities[a]	*N*[b]	mean (Å)	range (Å)
Pd(A)−Pd(B)	3	2.75	2.759(3)−2.734(3)
Pd(B)−Pd(B)	3	2.78	2.792(3)−2.770(3)
Pd(B)−Pd(D)	6	2.70	2.709(3)−2.685(3)
Pd(B)−Pd(E)	3	2.82	2.827(3)−2.798(3)
Pd(C)−Pd(D)	6	2.78	2.811(3)−2.766(3)
Pd(D)−Pd(D)	3	2.75	2.772(3)−2.720(3)
Pd(C)−br Pd(D)−Pd(D)	3	2.84	2.840(3)−2.842(3)
Pd(D)−Pd(E)	6	2.80	2.819(3)−2.778(3)
Pd(C)−Pd(F)	3	3.19	3.212(3)−3.151(3)
Pd(C)−Pd(G)	6	2.86	2.913(3)−2.829(3)
Pd(D)−Pd(G)	6	2.82	2.858(3)−2.781(3)
Pd(D)−Pd(I)	6	2.89	2.825(3)−2.853(3)
Pd(D)−Pd(H)	6	2.83	2.967(3)−2.905(3)
Pd(E)−Pd(I)	3	2.75	2.750(3)−2.747(3)
Pd(F)−Pd(G)	6	2.72	2.749(3)−2.700(3)
Pd(G)−Pd(G)	3	2.91	2.927(3)−2.882(3)
Pd(G)−Pd(H)	6	2.73	2.757(3)−2.697(3)
Pd(G)−Pd(I)	6	2.80	2.836(3)−2.767(3)
Pd(H)−Pd(I)	6	2.92	2.944(3)−2.867(3)
Pd(I)−Pd(I)	3	2.76	2.775(3)−2.739(3)
mean Pd−Pd	87	2.82	3.212(3)−2.685(3)
Pd(A)-P(1)	1	2.31	2.314(8)
Pd(C)−P(2)	3	2.34	2.354(8)−2.329(8)
Pd(F)−P(3)	3	2.33	2.335(8)−2.316(8)
mean Pd−P	7	2.33	2.354(8)−2.314(8)

[a] Atom-labeling for the metal core is given in Figure 8. [b] *N* denotes the number of symmetry-equivalent metal−metal and Pd−P connectivities under C_{3v} symmetry.

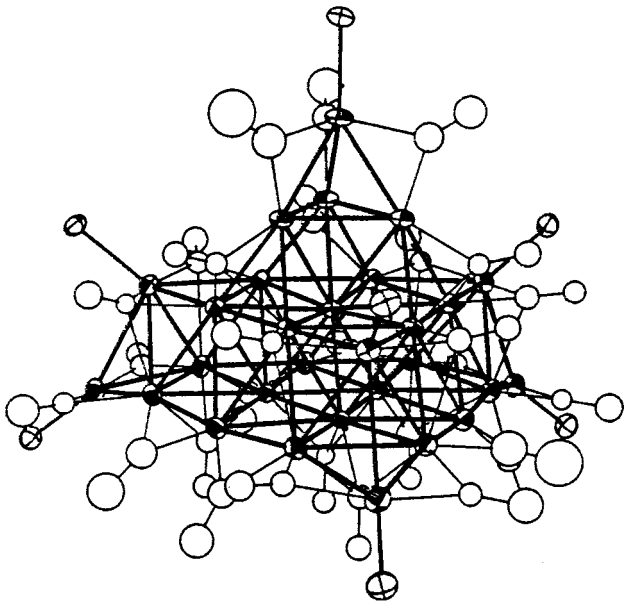

Figure 9. Configuration of $[Pd_{29}(\mu_2\text{-}CO)_{15}(\mu_3\text{-}CO)_{13}(PPh_3)_7]^{2-}$ (**4**) without the phenyl substituents. The connectivities of the triphenyl phosphine P atoms and 28 bridging carbonyl ligands about the four-layer Pd_{29} core preserve the pseudo-C_{3v} symmetry.

third layer. This 10-atom third layer is connected to the 15-atom fourth (bottom) layer by six triply bridging COs; each one caps a triangular corner atom in the fourth layer with a triangular corner atom and an adjacent interior atom along one of the three 5-atom edges of the fourth layer. Only this bottom layer has doubly and triply bridging *intralayer* COs. These consist of 12 doubly bridging COs which edge-bridge the four pairs of five atoms along each edge and four triply bridging COs, of which one caps the central palladium triangle and the remaining three each cap one of the central atoms and two

adjacent interior atoms on different edges. This carbonyl distribution is consistent with its IR spectrum which exhibits absorption bands only in the bridging CO region. The pseudo 3-fold axis in **4** passes through the top layer Pd(ap) atom and its attached phosphorus atom, the one interior Pd(i), and the triply bridging CO that caps the central palladium triangle in the bottom layer.

The observed number of CVEs for **4** is 362 (i.e., 29 × 10-(Pd) + 28 × 2(CO) + 7 × 2(PPh_3) + 2(charge) = 362). This number is in exact agreenent with that predicted from each of the three electron-counting models.[36,38,40]

The particular four-layer stacking sequence of the metal core in **4** is highly unusual for close-packed metal clusters in that the stacking of the 3-atom second layer to the 10-atom third layer results in a nonconvex polyhedron (Figure 8). This 29-atom metal architecture apparently originates from a stacking disorder that results in a mixed hcp/ccp arrangement. The interior Pd(i) atom in the third layer is at the center of a cuboctahedron which corresponds to a ccp sequence for the second, third, and fourth layers. If the top layer Pd(ap) atom were removed and if the Pd_3 triangle in the second layer were concomitantly expanded to a ν_2 Pd_6 triangle by Pd-capping of the three top "free" square faces of the cuboctahedron, a 31-atom truncated ν_4 palladium tetrahedron would then be formed. The additional face-fusion of a 7-atom monocapped octahedron to the inner triangle of the ν_2 Pd_6 triangle would result in a regular 35-atom ν_4 tetrahedron of cubic T_d symmetry, for which there are as yet no examples. It should be noted that the 30-atom ccp metal-core geometry crystallographically determined (and tentatively formulated as a $Pd_{16}Ni_{14}$ core) by Bacon[31] represents an edge-truncation of this same polyhedron (vide supra).

Synthesis and Reactions of $[Pd_{16}Ni_4(CO)_{22}(PPh_3)_4]^{2-}$ (1) and $[Pd_{33}Ni_9(CO)_{41}(PPh_3)_6]^{4-}$ (2). Both **1** and **2** were the major products isolated as $[PPh_4]^+$ salts in yields as high as 63% and 24%, respectively, by the slow addition of $PdCl_2(PPh_3)_2$ to $[Ni_6(CO)_{12}]^{2-}$ at room temperature in a DMSO/CH_2Cl_2 mixture. Optimization of the yields resulted in a 1:2 ratio of $PdCl_2(PPh_3)_2$ to $[Ni_6(CO)_{12}]^{2-}$ being used. PPh_4Br was added to the reaction solution and deoxygenated water was then added to the ice-cooled solution to crash out a black solid. An acetone extraction from the resulting black solid was used to isolate **1** along with an unidentified nickel species (vide infra). A relatively pure sample of **2** suitable for elemental analysis was isolated from the acetonitrile extract. Both **1** and **2** are *not* stable in acetonitrile solution, as indicated from UV−vis, NMR, and CV measurements. Microcrystalline samples of **1** and **2** were obtained via the layering of diisopropyl ether over an acetonitrile solution of **1** or **2**. Both clusters possess greater stability in polar organic solvents in the presence of excess electrolytes.

Because the closest-packed geometries of both **1** and **2** possess octahedral holes, it was initially presumed that these anions might "house" hydrogen atoms internally in a similar fashion as was found for ccp palladium metal which is currently used for commercial storage of tritium atoms.[6] Consequently, hydrogen-uptake and protonation reactions were carried out. The hydrogen-uptake experiments resulted in black precipitates that were insoluble in any solvent. Protonation reactions of separate microcrystalline samples of **1** and **2** with acetic acid in acetonitrile afforded in each case a few crystals which were crystallographically analyzed as the structurally important neutral $Pd_{12}(\mu_2\text{-}CO)_6(\mu_3\text{-}CO)_6(PPh_3)_6$ (**3**) and $[Pd_{29}(\mu_2\text{-}CO)_{15}(\mu_3\text{-}CO)_{13}(PPh_3)_7]^{2-}$ dianion (**4**), respectively. The acid-leaching of Ni atoms from the bimetallic **1** and **2** to give these homopalladium clusters is not surprising in light of Ni being similarly leached by acid from a zeolite-embedded Pd−Ni alloy.[14]

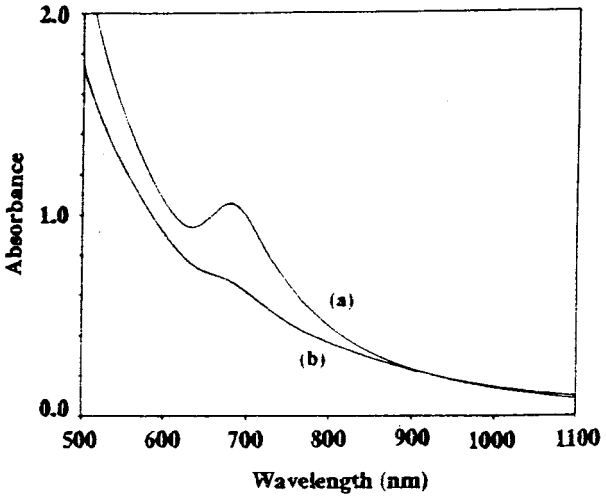

Figure 10. (a) UV−vis. solution spectrum of $[Pd_{16}Ni_4(CO)_{22}(PPh_3)_4]^{2-}$ (**1**) as $[PPh_4]^+$ salt in acetonitrile solution containing 0.1 M [n-Bu_4N]-[PF_6] electrolyte; each of 10 scans taken at 1.0 h intervals exhibited essentially no changes in the spectrum. (b) CV−vis. solution spectrum of $[Pd_{33}Ni_9(CO)_{41}(PPh_3)_6]^{4-}$ (**2**) as $[PPh_4]^+$ salt in acetonitrile solution containing 0.1 M [n-Bu_4N][PF_6] electrolyte; each of 12 scans taken at 1.0 h intervals showed essentially no changes in the spectrum.

Physical Properties of $[Pd_{16}Ni_4(CO)_{22}(PPh_3)_4]^{2-}$ (1) and $[Pd_{33}Ni_9(CO)_{41}(PPh_3)_6]^{4-}$ (2) and Resulting Implications. (a) Infrared Spectral Analysis. IR spectra of **1** and **2** in acetonitrile solution exhibit bands in the carbonyl stretching region that are *not inconsistent* with the solid-state geometries of **1** and **2**. For **1** the medium carbonyl band at 2002 cm^{-1} is assigned to the four Pd-attached terminal COs. The very strong carbonyl band at 1883 cm^{-1} and medium one at 1826 cm^{-1} are attributed to the 18 edge-bridged COs, of which 12 link Ni−Pd connectivities and the other six Pd−Pd connectivities. For **2** the single strong band at 1998 cm^{-1} is assigned to the five terminal COs, while the very strong, broad asymmetric band at 1883 cm^{-1} is assigned to the 24 edge-bridged COs.

No lower-frequency carbonyl band characteristic of the 12 face-bridging COs in **2** was observed. Such bands are usually weak, and often are not detected in solution IR spectra of other metal carbonyl clusters containing triply bridging carbonyl ligands.[67,68] The analogous terminal and bridging carbonyl frequencies observed in the IR spectra of **1** and **2** are consistent with similar negative charges being localized on the surface metal atoms in both clusters (i.e., the −2 charge being distributed over 20 surface metal atoms in **1** versus the −4 charge being distributed over 40 surface metal atoms in **2**).

(b) UV−Vis Spectral Analysis. The UV−vis solution spectra of **1** and **2** in 0.1 M [n-Bu_4N][PF_6] acetonitrile solution are shown in Figure 10. Both of these electronic spectra, which exhibit a broad, continuous electronic absorption characteristic of *interband* transitions, are typical for high-nuclearity metal carbonyl clusters.[3f] The solution spectrum of **1** (Figure 10) exhibits a well-defined band (above the interband absorption) with a maximum at ca. 680 nm, while that of **2** displays a small but discernible "bump" at the analogous wavelength above its interband absorption. Because the electronic origin of this band is unclear, no assignment is made at this time.

(67) (a) Cruz, C. D. L.; Sheppard, N. *J. Mol. Struct.* **1990**, *224*, 141 and references therein. (b) Kettle, S. F. A.; Diana, E.; Rossetti, R.; Stanghellini, P. L. *Inorg. Chem.* **1998**, *37*, 6502.

(68) (a) Mlynek, P. D.; Dahl, L. F. *Organometallics* **1997**, *16*, 1641. (b) Mlynek, P. D.; Dahl, L. F. *Organometallics* **1997**, *16*, 1655.

(c) NMR Spectral Analysis. Room-temperature $^{31}P\{^1H\}$ NMR spectra (500 MHz; 85% H_3PO_4, external) of **1** and **2** as $[PPh_4]^+$ salts in CD_3CN solutions each displayed a single phosphorus signal at δ 37.84 and δ 38.36 ppm, respectively. These single resonances for each of the anions are in accordance with their solid-state structures, each of which contains chemically equivalent phosphorus atoms. An identical signal at δ 21.78 ppm was observed in both spectra for the $[PPh_4]^+$ counterions of **1** and **2**. ^1H NMR spectra (500 MHz; CD_3CN at 23 °C) of **1** and **2** showed multiplets at 7.6−8.0 ppm for the phenyl protons of $[PPh_4]^+$ and PPh_3. No high-field signals corresponding to hydride atoms were detected; moreover, no paramagnetic shifts of the phenyl proton resonances of PPh_3 were observed.

(d) Cyclic Voltammetric Analysis. CVs of **1** and **2** (as $[PPh_4]^+$ salts) in acetonitrile solution do not exhibit any reversible redox behavior over a +2.0 to −2.0 V window (E vs SCE). CVs of **1** and **2**, respectively, in a 0.1 M $[n\text{-}Bu_4N][PF_6]$ acetonitrile solution at a platinum electrode with scan rates of 100 mV/s displayed analogous irreversible reduction waves at −0.55 V for **1** and −0.60 V for **2** and at least two irreversible oxidation waves at +0.20 and +0. 96 V for **1** and +0.40 and +1.00 V for **2**.

This irreversible electron-transfer behavior is in distinct opposition to a number of high-nuclearity platinum and Pt−Ni carbonyl clusters that show multiple reversible CV waves characteristic of sequences of multiple charged anions that exist without rupture of their platinum cluster cores.[17b,69] This prime evidence for the nonexistence of other electroactive charged anions of **1** and **2** is attributed to the much smaller cohesive energies of Pd−Pd and Pd−Ni bonding (relative to that of Pt−Pt bonding in these close-packed metal clusters)[46,47] not allowing reversible redox changes to occur without metal-core breakdown.

(e) Magnetic Susceptibility Analysis. No evidence of paramagnetism in either **1** or **2** (as $[PPh_4]^+$ salts) was detected over the entire temperature range from 5.0 to 300 K. It is not surprising that the magnetic susceptibility measurements revealed no evidence of any paramagnetism. Compound **1** does not contain any internal metal atoms, while **2** has a single internal Pd(i) atom.

Local density function (LDF) calculations and experimental single-crystal magnetization studies on $[H_2Ni_{12}(CO)_{21}]^{2-}$ (as the $[NMe_3Bz]^+$ salt) and $[HPt_6Ni_{38}(CO)_{48}]^{5-}$ (as the mixed $2[AsPh_4]^+/3[NBu_4]^{2+}$ salt) provide convincing evidence that the effect of carbonyl ligation completely quenches the magnetic moments of the surface Ni(s) atoms in both compounds.[70,71] The Ni_{12} cluster has only surface Ni(s) atoms, while the Pt_6Ni_{38} cluster is composed of an interior $Pt(i)_6$ octahedron enclosed in an outer octahedron of 38 surface Ni(s) atoms. The magnetization of each compound was measured via a SQUID magnetometer as a function of field (up to 6 T) and temperature (1.7−300 K). From the experimental results it was concluded for the HPt_6Ni_{38} carbonyl cluster that the six interior Pt(i) atoms are also nonmagnetic. Similar surface-quenching magnetic effects due to ligation were likewise found in an experimental study of the size-dependent magnetization of giant Pd clusters and Pd colloids.[71,72]

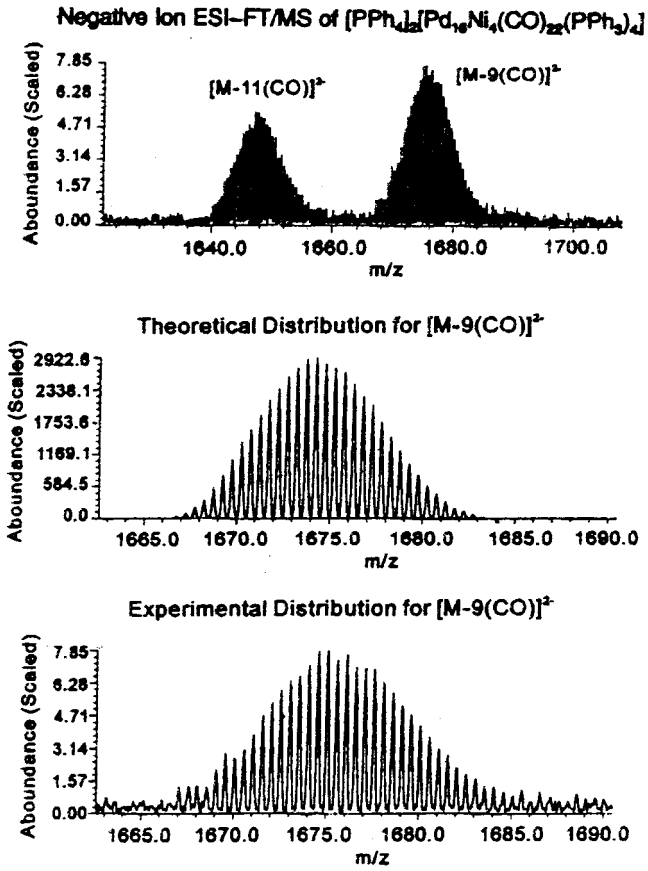

Figure 11. Negative-ion ESI FT/ICR mass spectrum of $[Pd_{16}Ni_4(CO)_{22}(PPh_3)_4]^{2-}$ (**1**) as $[PPh_4]^+$ salt in dilute (ca. 10^{-4} M) acetonitrile solution. The top picture displays the mass spectrum of two prominent signals at 1674.5 and 1646.5 amu corresponding to doubly charged $[M\text{-}(CO)_9]^{2-}$ and $[M\text{-}(CO)_{11}]^{2-}$ fragment-ions, respectively, where M denotes the parent-ion **2**. The experimental isotopic distribution pattern corresponding to the $[M\text{-}(CO)_9]^{2-}$ fragment-ion (bottom picture) matches closely with its theoretical isotopic distribution pattern (middle picture).

(f) Mass Spectrometry Analysis. A negative-ion mass spectrum of $[PPh_4]_2[Pd_{16}Ni_4(CO)_{22}(PPh_3)_4]$ exhibited high-range *m*/*z* signals corresponding to doubly charged fragment-ions. Although the doubly charged parent-ion, $[Pd_{16}Ni_4(CO)_{22}(PPh_3)_4]^{2-}$, denoted as M^{2-} was not detected, several observed signals correspond to $[M\text{-}(CO)_n]^{2-}$ ions (n = 6, 7, 8, 9, 11). Figure 11 displays the experimental signals at 1674.5 and 1646.5 amu that were assigned to the $[M\text{-}(CO)_9]^{2-}$ and $[M\text{-}(CO)_{11}]^{2-}$ fragment-ions, respectively, along with a comparison of the observed isotopic distribution pattern for $[M\text{-}(CO)_9]^{2-}$ with its simulated pattern for the assigned signal. The close matching clearly indicates the bimetallic core, $Pd_{16}Ni_4$, in **1**. It is not surprising that the parent-ion M^{2-} signal was not detected, because in general metal carbonyl compounds readily lose carbonyl ligands in the process of ionization in a mass spectrometer.

In the case of ESI FT/MS, fragmentation depends on the capillary skimmer voltage (CSV) difference. The experimental signals displayed in Figure 11 for **1** correspond to a CSV difference of 60 V. When the CSV difference was increased to 100 V, the signal for $[M\text{-}(CO)_9]^{2-}$ decreased while that for

(69) (a) Lewis, G. J.; Roth, J. D.; Montag, R. A.; Safford, L. K.; Gao, X.; Chang, S.-C.; Dahl, L. F.; Weaver, M. J. *J. Am. Chem. Soc.* **1990**, *112*, 2831. (b) Roth, J. D.; Lewis, G. J.; Safford, L. K.; Jiang, X.; Dahl, L. F.; Weaver, M. J. *J. Am. Chem. Soc.* **1992**, *114*, 6159.

(70) (a) van Leeuwen, D. A.; van Ruitenbeek, J. M.; de Jongh, L. J.; Ceriotti, A.; Pacchioni, G.; Häberlen, O. D.; Rösch, N. *Phys. Rev. Lett.* **1994**, *73*, 1432. (b) Pacchioni, G.; Rösch, N. *Acc. Chem. Res.* **1995**, *28*, 390 and references therein.

(71) de Jongh, L. J. *Appl. Organomet. Chem.* **1998**, *12*, 393 and references therein.

(72) van Leeuwen, D. A.; van Ruitenbeek, J. M.; Schmid, G.; de Jongh, L. J. *Phys. Lett. A* **1992**, *170*, 333.

$[M\text{-}(CO)_{11}]^{2-}$ increased such that the relative fragment-ion abundances (intensities) of these two signals were opposite from those shown in Figure 11; this experimental change indicates that the higher CSV difference accelerated the decarbonylation of the M^{2-} parent-ion. We were previously unsuccessful in obtaining a mass spectrum of **1** with a FAB MS spectrometer. These results provide a striking illustration of the immense capability of the ESI process in placing a nonvolatile metal carbonyl cluster anion into the gas phase generally with little or no fragmentation (other than expected loss of CO ligands) for mass spectral analysis.

Attempts to obtain corresponding mass spectral data for **2** (as the $[PPh_4]^+_4$ salt) were not successful presumably due to its greater instability in dilute acetonitrile solution (i.e., ca. 10^{-4} M). Even **1** undergoes slow decomposition, despite special precautions being taken in sample preparations (i.e., deoxygenated solutions were prepared just prior to each measurement).

Experimental Section

Materials and General Procedures. All reactions and manipulations were carried out under an atmosphere of nitrogen via standard Schlenk techniques, in a glovebag, or in a Vacuum Atmospheres glovebox. The following solvents were dried and distilled prior to use: CH_3CN (CaH_2), acetone ($CaSO_4$), CH_3OH (Mg), THF (potassium/benzophenone ketyl), CH_2Cl_2 (CaH_2), diisopropyl ether (potassium/benzophenone ketyl), and hexane (CaH_2). Anhydrous Et_2O (0.004% H_2O, Mallinckrodt) and acetic acid (99.7%, EM SCIENCE) were used without further purification. $[Me_4N]^+_2[Ni_6(CO)_{12}]^{2-}$ was prepared by minor modifications of the procedure described by Longoni, Chini, Ceriotti, and co-workers.[73]

Infrared spectra were recorded on either a Mattson Polaris FT-IR or a Nicolet 740 FT-IR spectrophotometer. Solution spectra were obtained by use of nitrogen-purged CaF_2 cells. The carbonyl frequencies reported were observed in the 1600 to 2200 cm^{-1} window. UV−vis spectra were recorded on either a HP 8452 Diode Array Spectrophotometer or a PERKIN ELMER UV/VIS Spectrometer Lambda 20. Cyclic voltammograms were obtained with BAS-100 Electrochemical Analyzer with the electrochemical cell enclosed in a nitrogen-filled Vacuum Atmospheres glovebox. Electrochemical measurements were carried out in acetonitrile containing 0.1 M [n-Bu_4N][PF_6] (Fluka). The working electrode was a platinum disk, and the reference electrode was a Vycor-tipped aqueous SCE separated from the test solution by a Vycor-tipped salt bridge filled with a 0.1 M [n-Bu_4N] [PF_6]/CH_3CN solution. The auxiliary electrode was a platinum wire.

All ^1H and $^{31}P\{^1H\}$ NMR spectra were recorded on a Bruker AM-500 spectrometer; chemical shifts are reported relative to Me_4Si calculated from the chemical shifts of residual solvent protons and with phosphoric acid as an external reference, respectively.

Mass spectra were obtained by B. E. W. on a the NewStar high-resolution FT/MS 2001 mass spectrometer (Finnigan FT/MS Corp., Madison, WI) with an electrospray ionization technique. A freshly prepared sample of **1** was injected as a acetonitrile solution under inert atmosphere at 10 μL/min. The capillary skimmer voltage difference was 60 V.

Crystalline samples of **1** and **2** were examined via ac susceptiility measurements carried out by J.D.D., S.A.S., S.L.S., and U.G. at Argonne National Laboratory. Data were collected with a Lake Shore Cryotronics 7221 ac susceptometer operated with a 1G modulation field, and a frequency of 125 Hz. Samples were cooled in zero field over a time period of 15 min. Magnetic susceptibility data were recorded from 5.0 to 300 K as the sample was warmed in 0.1 K increments.

Preparation of $[Pd_{16}Ni_4(CO)_{22}(PPh_3)_4]^{2-}$ (1) and $[Pd_{33}Ni_9(CO)_{41}(PPh_3)_6]^{4-}$ (2) as $[PPh_4]^+$ Salts. A slurry of 0.83 g (1.18 mmol) of $PdCl_2(PPh_3)_2$ in 20 mL of DMSO and 5 mL of CH_2Cl_2 was slowly dripped over a 15−20 min period into a solution of 0.50 g (0.60 mmol) of $(Me_4N)_2[Ni_6(CO)_{12}]$ in 15 mL of DMSO at room temperature. During this time the solution turned from dark red to dark yellowish brown. After the solution was stirred for 5 h CH_2Cl_2 and CO were removed under a nitrogen purge. Stirring was continued for an additional 7 h, after which 3.50 g (8.35 mmol) of Ph_4PBr in 50∼60 mL of CH_3OH was added to the solution. To precipitate the products, 80 mL of water was then slowly added while the solution was cooled with an ice bath. After filtration, the black product was washed with H_2O (1 × 30 mL), CH_3OH (2 × 50 mL), and THF (3 × 50 mL) mainly in order to remove excess Ph_4PBr, free PPh_3, $OPPh_3$, and unreacted $[Ni_6(CO)_{12}]^{2-}$ dianion. After extraction with acetone (2 × 60 mL), the solvent was then removed under a nitrogen purge. The resulting solid was washed with CH_3OH (3 × 30 mL), THF (3 × 30 mL), and hexane (3 × 20 mL). $[PPh_4]^+_2[Pd_{16}Ni_4(CO)_{22}(PPh_3)_4]^{2-}$ (0.20 g, 63% yield based on $PdCl_2(PPh_3)_2$) was obtained as a black powder from the acetone extraction. The elemental analysis (vide infra) indicated an unknown Ni contaminant, which had not separated from **1** in the solvent extractions.

After the acetone extraction, the original black product was extracted with acetonitrile (2 × 20 mL). The solvent was removed under a nitrogen purge, and some crystals appeared. The microcrystalline product was washed sequentially with CH_3OH (3 × 30 mL), THF (3 × 30 mL), and hexane (3 × 20 mL). $[PPh_4]^+_2[Pd_{33}Ni_9(CO)_{41}(PPh_3)_6]^{4-}$ (0.07 g, 24% yield based on $PdCl_2(PPh_3)_2$), was obtained as a black microcrystalline product from the acetonitrile extraction. After the acetone and acetonitrile extractions, a small amount of insoluble black powder remained.

Other starting materials, $PdCl_2(PR_3)_2$ (R = Me, Et, OMe), were used in place of $PdCl_2(PPh_3)_2$. Although each of these palladium precursors reacted with $[Me_4N]_2[Ni_6(CO)_{12}]$ to give dark brown solutions, only unidentified black powders were obtained.

Elementary analyses were performed by Desert Analytics (Tucson, AZ) on three different samples of **1** and one sample of **2** (as $[PPh_4]^+$ salts).

Anal. Calcd for $[Ph_4P]_2[Pd_{16}Ni_4(CO)_{22}(PPh_3)_4]\cdot CH_3CN$ (fw = 4322.76). C, 40.01; H, 2.40; N, 0.32; Ni, 5.43; Pd, 39.39. Found for first sample: C, 37.42; H, 2.48; N, 0.82; Ni, 12.76; Pd, 39.04. Found for second sample: C, 36.07; H, 2.17; N, 0.04; Ni, 11.03; Pd, 41.23. Found for third sample: C, 40.17; H, 2.37; N, 0.18; Ni, 5.50; Pd, 39.71. Analyses of the first two microcrystalline samples of **1** gave much higher percentages of Ni than the calculated percentage (viz, 12.76% and 11.03% versus 5.43%); this difference indicated an unknown Ni contaminant. Consequently, large single crystals were used for the third sample, from which the resulting elemental analysis exhibited good agreement between the experimental and calculated pearcentages for all elements including Ni.

Anal. for $[Ph_4P]_4[Pd_{33}Ni_9(CO)_{41}(PPh_3)_6]\cdot CH_3CN$ (fw = 8160.97) Calcd (found): C, 36.35 (36.16); H, 2.14 (2.40); N, 0.17 (0.26); Ni, 6.47 (6.75); Pd, 43.03 (46.57). The good agreement between the calculated and observed percentages for each element in the acetonitrile-solvated $[PPh_4]^+$ salt of **2** indicated that the microcrystalline product obtained from the acetonitrile extraction was relatively pure.

Reaction of $[Pd_{16}Ni_4(CO)_{22}(PPh_3)_4]^{2-}$ (1) with Acetic Acid. In a typical reaction, 5 mL of AcOH was added to a stirred solution of the powder sample of **1** (0.21 g, 0.05 mmol) in 15 mL of acetonitrile. Within 10 min, the solution yielded a brown precipitate. After 16 h the acetonitrile solution was removed by a N_2 purge; the remaining AcOH solution was filtered. The resulting dark solid was washed with water (2 × 10 mL). After the solid was extracted with CH_3OH (2 × 20 mL), a dark brown powder remained. An attempted crystallization of the brown methanol extract from acetonitrile/Et_2O gave 0.04 mg of a powder. A THF extraction (2 × 20 mL) resulted in a light brown solution. The dark brown powder was extracted from acetone (2 × 20 mL). This latter extract was reduced to 10 mL by a N_2 purge and then crystallized by a layering diffusion of Et_2O. Approximately 0.10 g of the product included the mixture of a few crystals and a dark brown powder. The molecular formula of $Pd_{12}(CO)_{12}(PPh_3)_6$ (**3**) was established from the X-ray crystallographic analysis. Since $Pd_{12}(CO)_{12}(PPh_3)_6$ was obtained in extremely low yields in this reaction, no further analysis was carried out.

Reaction of $[Pd_{33}Ni_9(CO)_{41}(PPh_3)_6]^{4-}$ (2) with Acetic Acid. In a typical reaction, 5 mL of AcOH was added to a stirred solution of a powder sample of **2** (0.07 g, 0.009 mmol) in 15 mL of acetonitrile. After addition the solution immediately produced a brown precipitate.

(73) (a) Longoni, G.; Chini, P.; Cavalieri, A. *Inorg. Chem.* **1976**, *15*, 3025. (b) Ceriotti, A.; Longoni, G.; Piva, G. *Inorg. Synth.* **1989**, *26*, 312.

Table 5. Crystallographic Data and Refinement Parameters for $[Ph_4P]^+_2[Pd_{16}Ni_4(CO)_{22}(PPh_3)_4]^{2-}$ (**1**), $[Ph_4P]^+_4[Pd_{33}Ni_9(CO)_{41}(PPh_3)_6]^{4-}$ (**2**), $Pd_{12}(CO)_{12}(PPh_3)_6$ (**3**), and $[Ph_4P]^+_2[Pd_{29}(CO)_{28}(PPh_3)_7]^{2-}$ (**4**)

	1·2MeCN·1.64Me_2CO·0.64*i*-Pr_2O	**2**·3MeCN·5Me_2CO	**3**·2(Me_2CO)	**4**·3(MeCN)
fw	4524.46	8526.65	3302.70	6507.67
cryst syst	orthorhombic	monoclinic	monoclinic	triclinic
space group	$P2_12_12_1$	$C2/c$	$P2_1/n$	$P\bar{1}$
a (Å)	18.5409(4)	22.761(2)	14.1712(1)	20.5934(1)
b (Å)	28.0697(6)	29.584(2)	23.8035(2)	21.0563(3)
c (Å)	30.2282(7)	40.844(3)	18.8776(1)	28.3899(4)
α (deg)				82.367(1)
β (deg)		102.213(3)	109.863(1)	79.800(1)
γ (deg)				67.029(1)
V (Å)^3	15731.9(6)	26881(3)	5989.03(7)	11127.5(2)
Z	4	4	2	2
ρ_{calcd} (g/cm^3)	1.910	2.107	1.831	1.942
μ (Mo Kα) (mm^{-1})	2.369	2.885	1.895	2.401
data collectn temp (K)	133(2)	296(2)	133(2)	188(2)
crytal size (mm)	0.45 × 0.20 × 0.20	0.20 × 0.10 × 0.10	0.20 × 0.20 × 0.20	0.40 × 0.20 × 0.10
no. of unique data	24178	19366	10652	25512
no. of parameters	1891	1605	884	2087
weighting scheme a, b[a]	0.0344, 202.6558	0.0000, 1463.36	0.0343, 0.0000	0.0333, 896.5696
goodness-of-fit on F^2	1.102	1.288	0.936	1.111
final R indices [F 4$\sigma(F)$][b]	$R1 = 0.0632$, w$R2 = 0.1406$	0.0882, 0.1536	0.0499, 0.0948	0.1136, 0.2404
R indices (all data)[b]	$R1 = 0.0742$, w$R2 = 0.1498$	0.1193, 0.1714	0.0864, 0.1046	0.1450, 0.2792
largest and mean Δ/esd	−0.012, 0.001	−0.001, 0.000	0.004, 0.000	0.017, 0.000

[b] $w = I/[\sigma^2(F_o^2) + (a \times P)^2 + b \times P]$; $P = [F_o^2 + (2F_c^2)]/3$. [b] $R1(F) = \sum||F_o| - |F_c||/\sum|F_o|$; $wR2(F^2) = [\sum w_i(F_o^2 - F_c^2)^2]/\sum[w_i(F_o^2)^2]]^{1/2}$.

After 3 h, the acetonitrile solution was removed by a N_2 purge; the remaining AcOH solution was filtered. The resulting dark solid was washed with water (2 × 10 mL) and methanol (2 × 20 mL), leaving behind a dark brown powder. THF extraction (2 × 20 mL) produced a brown solution. An attempted crystallization of the THF extract with i-Pr_2O resulted in a powder sample. A dark brown powder was first extracted from acetone (10 mL) and then acetonitrile (10 mL). The extract was reduced into 10 mL by N_2 purge, after which a layering diffusion of i-Pr_2O gave a powder along with a few leaf-shape thin crystals. Characterization of the crystals by an X-ray diffraction analysis unequivocally revealed them to be $[Ph_4P]_2[Pd_{29}(CO)_{28}(PPh_3)_7]$. Because this compound was obtained only in very low yields, no further work was carried out. IR (acetonitrile, CaF_2) ν(CO), cm^{-1}: 1917 (s), 1897 (s), 1882 (w, sh), 1846 (w).

X-ray Crystallographic Analyses. (a) General Procedures. Intensity data for each compound were collected via a SMART CCD area detector mounted on a Bruker P4 diffractometer with graphite-monochromated Mo Kα radiation from a sealed-tube generator. An empirical absorption correction (SADABS) was applied to each data set. Structural determinations were obtained from direct methods. Anisotropic least-squares refinements (based on F^2) were carried out with SHEXTL (version 5, 1994). Crystal data, data-collection, and refinement parameters for each of the four compounds are given in Table 5.

(a) $[PPh_4]^+_2[Pd_{16}Ni_4(CO)_{22}(PPh_3)_4]^{2-}$·2 MeCN·1.64 Me_2CO·0.64 i-Pr_2O. Suitable untwinned black crystals for X-ray diffraction analysis were finally obtained via a layering-diffusion of diisopropyl ether into an acetone−acetonitrile solution. Least-squares refinement under orthorhombic $P2_12_12_1$ symmetry resulted in the above crystallographically independent formula involving orientationally disordered acetone/diisopropyl ether molecules. A crystal-disorder was also observed for one of the two independent $[PPh_4]^+$ counterions; the refined occupancy-factor ratio was 0.65/0.35 for this cation being distributed over two slightly displaced positions in the average unit cell, presumably resulting from different steric effects of the disordered solvated acetone/diisopropyl ether molecules. However, no crystal-disorder was observed for the dianion (**1**).

A layering-diffusion of diisopropyl ether into an acetonitrile solution invariably gave block-shaped twinned crystals of monoclinic $P2_1/c$ symmetry. Crystallizations of **1** with either $[N(n\text{-}Bu)_4]^+$ or $[NEt_4]^+$ cations gave poor-quality crystals. In most crystallizations, twinned or multicrystals were easily obtained. To obtain single crystals, extra caution was taken to avoid solution vibration during crystallization.

(b) $[PPh_4]^+_2[Pd_{33}Ni_9(CO)_{41}(PPh_3)_6]^{4-}$·3MeCN·5$Me_2CO$. Black crystals were obtained from an acetone/acetonitrile solution via a layer-diffusion with diisopropyl ether. The crystallographically independent unit consists of two $[PPh_4]^+$ cations, one-half of the tetraanion (**2**) lying on a 2-fold axis, and orientationally disordered acetonitrile/diisopropyl ether molecules.

(c) $Pd_{12}(\mu_2\text{-}CO)_6(\mu_3\text{-}CO)_6(PPh_3)_6$·2$Me_2CO$. A few black crystals of neutral **3** were isolated from a layering-diffusion of diethyl ether into an acetone solution. The crystallographically independent unit is composed of one-half of **3** located on an inversion center and one acetone molecule.

(d) $[PPh_4]^+_2[Pd_{29}(CO)_{28}(PPh_3)_7]^{2-}$·3MeCN. A few black crystals were isolated from a layering-diffusion of diisopropyl ether into an acetone/acetonitrile solution. The crystallographically independent unit is comprised of two $[PPh_4]^+$ cations, one dianion (**4**), and three acetonitrile molecules.

Acknowledgment. The research at UW-Madison was supported by the National Science Foundation (Grants CHE-9310428 and CHE-9729555). Departmental purchase of the CCD area detector system in 1995 was made possible by funds from NSF (Grant CHE-9310428) and the UW-Madison Graduate School and Chemistry Department. The variable-temperature magnetic susceptibility work is sponsored by the U. S. Department of Energy, Office of Basic Energy Sciences, Division of Materials Sciences, under Contract W-31-109-EWG-38. S.A.S. and S.L.S. were student undergraduate research participants, sponsored by the Argonne Division of Educational Programs, from Mansfield University (Mansfield, PA) and Alabama A&M University (Normal, AL), respectively. We are grateful to Finnigan FT/MS Corporation (no longer in Madison, WI) for the use of their New-Star high-resolution FT/MS 2001 mass spectrometer and its electrospray ionization source. We also thank Dr. Douglas Powell (UW-Madison) for helpful crystallographic advice and Dr. Nguyet T. Tran for her indispensable assistance in the preparation of this manuscript.

Note Added in Proof. Dr. Eugeny Mednikov, currently a visiting senior scientist with our group at UW—Madison (from the Institute of Coal and Coal Chemistry, Siberian Branch of Russian Academy of Sciences, Kemerovo, Russia), recently provided conclusive evidence that the previously reported $Pd_8(CO)_{10}(PPh_3)_4$ (Mednikov, E. G.; Eremenko, N. K.; Hkivintseva, G. A. *Sov. J. Coord. Chem.* **1987**, *13*, 106 (in Russian)), which was initially formulated on the basis of elemental analysis

and IR, is actually $Pd_{12}(CO)_{12}(PPh_3)_6$ (**3**). An attempt in 1986 to determine the MW of this cluster from a freezing point depression study was unsuccessful due to its relative insolubility in all common organic solvents (viz., benzene, toluene, THF, acetone, DMF, and DMSO). Mednikov prepared the compound again at UW−Madison from the following original procedure: 25 mg (0.0084 mmol) of $Pd_{10}(CO)_{12}(PPh_3)_6$ and 7.7 mg (0.0084 mmol) of $Pd_2(dba)_3$ (where dba denotes dibenzylideneacetone) were dissolved in 6 mL of THF and 2 mL of Me_2CO under N_2. After 5 days, the reaction was terminated, and black blocklike crystals of $Pd_{12}(CO)_{12}(PPh_3)_6 \cdot 2Me_2CO$ were isolated. A CCD X-ray diffraction analysis showed that the unit-cell dimensions of one crystal were virtually identical with those reported herein for **3**·$2Me_2CO$ (Table 5). An IR spectrum (Nujol), which exhibited carbonyl bands at 1881 (vs), 1831 (s), 1799 (m), and 1789 (sh) cm^{-1}, was virtually identical with the previously given IR spectrum. Particularly noteworthy is that the percentages for all of the elements in the previously reported elemental analysis are in excellent agreement with those based upon the revised formula, $Pd_{12}(CO)_{12}(PPh_3)_6$ (**3**): Calcd (found): Pd, 40.07 (39.23); P, 5.83 (5.66); C 45.23 (44.92); H, 2.85 (2.93). Mednikov also prepared **3**·$0.5C_7H_8$ in similar high yields (ca. 70%) from reactions of $Pd_4(CO)_5(PPh_3)_4$ either with air in toluene or with $Pd(OAc)_2$ in toluene. We are greatly indebted to Dr. Mednikov for providing these highly informative results.

Supporting Information Available: Tables listing crystallographic data for the four compounds (PDF). This material is available free of charge via the Internet at http://pubs.acs.org.

IC000979P